Assessing and Mitigating Carbon Emission Exposure in Dynamic Multimodal Transport Networks

Yaxin Wu a, b, Xiaowei Hu a, *, Yujia Wang a, c, Yu Jiang b, d, *

^a School of Transportation Science and Engineering, Harbin Institute of Technology, Harbin, 150090, China

^b Lancaster University Management School (LUMS), Lancaster University, Lancaster, LA1 4YX, United Kingdom

^c Department of Aeronautical and Aviation Engineering, Faculty of Engineering, The Hong Kong Polytechnic University, Hong Kong SAR

^d Department of Management Engineering, Technical University of Department, Lyngby, 2800, Denmark

*Corresponding authors.

E-mail addresses: 21b932020@stu nit.edu.cn (Y. Wu), x1aowei hu@hit.edu.cn (X. Hu),

23041688r@connect.polyubl (Y. Wang), vujiang@lancaster.ac.uk (Y. Jiang).

Assessing and Mitigating Carbon Emission Exposure in Dynamic Multimodal Transport

Networks

Abstract

On-road carbon emissions from heterogeneous traffic flows in multimodal urban transportation systems pose a significant risk to public health. Developing effective instruments to mitigate these emissions requires accurate modelling and assessment of their impact on the environment. To this end, this study establishes a holistic framework that integrates two interrelated components: 1) a multimodal dynamic traffic assignment model for obtaining equilibrated flow distributions, and 2) a Gaussian plume model, underpinned by a multi-category vehicle carbon emission model, to assess the spatiotemporal distribution of exposure. Numerical experiments demonstrate the model convergence and evaluate its performance under multiple scenarios. Results show that incorporating the proposed carbon emission cost and exposure cost into dynamic traffic assignment can simultaneously reduce carbon emissions and exposure risks, underscoring the necessity of jointly considering both factors in path choice modeling to achieve sustainable urban mobility and the broader development of low-carbon, healthy cities.

Keywords: Carbon emission exposure; Dynamic traffic assignment; Heterogeneous flows; Multimodal transportation

1. Introduction

Urban transportation contributes up to 16% of worldwide greenhouse gases, ranking third in carbon dioxide (CO₂) emission sources (Lu et al., 2024). Exposure to emissions can cause a range of health problems, including heat-induced ailments, respiratory illnesses, and cardiovascular diseases (Mohsenizadeh et al., 2020; Burns et al., 2020; Dadashev et al., 2023). These impacts highlight the

need for measures that effectively reduce carbon emissions, addressing not only the total amount emitted but also the level of exposure.

Currently, there are two main approaches for reducing vehicle carbon emissions in urban road networks. From a technical perspective, one approach is to reduce vehicle emissions through measures such as improving fuel quality, promoting new energy vehicles, and enhancing tailpipe cleaning technologies (Shen et al., 2024). This approach primarily focuses on reducing emissions from individual vehicles; however, its effectiveness depends on the adoption and widespread market penetration of new technologies, which may require a prolonged timeframe. From a policy perspective, the other approach employs traffic demand management instruments to induce changes in travel behavior, such as shifting to green travel modes or adjusting travel times and routes (Kamishetty et al., 2020; Zeng et al., 2020; Djavadian et al., 2(2000), which could deliver substantial results within a comparatively short timeframe. In practice, key traffic management schemes implemented include traffic control (e.g., restrictions and bans) (Long et al., 2018; Song et al., 2020) and pricing (e.g. taxes, charges and tolls) (Zong et al., 2024). Comparatively, strategies that adjust travelers' path choices in conjunction with emission pricing are considered more effective in reducing overall emissions and exposure.

The design of emission pricing is commonly built upon traffic assignment models (e.g., Ma et al., 2017; Sharma and Mishra, 2011), which incorporate carbon emission costs as a disutlity that reduces the probability of a route being chosen. However, most existing studies focus primarily on aggregated emission quantities, while overlooking the spatiotemporal distribution of emissions and the associated health exposure of travellers. Moreover, only a limited number of studies (Fan et al., 2024; Xi et al., 2025) account for travel behaviour in a multimodal transport network, despite its growing prominence

in modern urban mobility contexts. Consequently, the complex relationships among travel time, emissions, and exposure remain insufficiently understood, leaving an inadequate foundation for developing pricing-based demand management measures in multimodal networks.

To bridge two major gaps, this study develops an integrated dynamic modeling framework that captures travel behavior, carbon emission, and exposure risk in multimodal networks. Specifically, we construct a multimodal dynamic traffic assignment (DTA) model that incorporates generalized travel cost, carbon emission cost, and exposure cost into travelers' route choices. Carbon emissions are estimated using a macroscopic emission model calibrated for different travel modes, while traveler exposure is quantified based on a Gaussian dispersion process that captures the spatiotemporal dispersion across the network. To solve the dynamic multimodal traffic assignment, the Method of Successive Averages (MSA) is employed. The proposed framework is applied to both a testing network and a real-world network to evaluate its performance and derive policy insights. Through scenario analysis, we examine how different cost configurations affect carbon emissions, exposure risks, and travel patterns, thereby revealing the trade-offs and synergies between environmental and health objectives in sustainable transportation planning.

This research contributes to the literature in the following ways:

- 1) It quantifies both carbon emissions and exposure, measured by their health impacts, in a multimodal transportation network.
- 2) It integrates both emission and exposure costs within the travel behaviour model, i.e., an extended multimodal DTA model incorporating multi-destination trips.
- 3) The results reveal the irreplaceable roles of both emission and exposure costs in traffic flow management, underscoring the necessity of addressing them jointly within the decision-making

framework.

The organization of this paper unfolds in the following manner. Section 2 delves into an examination of pertinent academic literature. Section 3 unveils the proposed modeling framework. Section 4 conducts a numerical analysis, interprets the findings, and extrapolates policy recommendations. Section 5 concludes this study and outlines avenues for future research.

2. Literature review

This section reviews the most relevant studies in two directions that underpin this research: (1) the spatiotemporal assessment of carbon emissions and their exposure impacts on travelers, and (2) the incorporation of environmental and health costs into dynamic path choice models.

2.1. Spatiotemporal analysis of travel behavior, carbon emissions and exposure

Many studies have quantified traffic-related carbon emissions using either macroscopic or microscopic approaches (He et al. 202%, Jia et al., 122). Macroscopic models estimate emissions based on aggregated speed—flow relationships (He et al. 2020), and are widely adopted due to their computational efficiency in large-scale networks. Recent studies have started integrating these models with DTA to capture temporal variations in traffic flow and emissions (Long et al., 2018; Pinto et al., 2020; Vosough et al., 2027, Mei and Liu, 2023). However, most of these efforts focus solely on emissions, without accounting for pollutant dispersion or their health impacts on travelers.

Traveler exposure to traffic-generated air pollutants is an increasingly pressing concern. Studies have used Gaussian dispersion models to simulate how pollutants spread from roadways (e.g., Liang et al., 2023), and some have linked emissions and exposure through dynamic simulations (e.g., Tan et al., 2021; Dadashev et al., 2023). However, most of these studies consider exposure passively

(Vosough et al., 2022). That is, exposure is typically estimated after path choices are made, rather than being treated as a factor influencing travel behavior itself. Moreover, although multimodal networks are increasingly recognised as integral to sustainable transportation, their role in this context remains largely underexplored.

This study contributes to this line of research by developing a framework that simultaneously models dynamic travel behavior, carbon emissions, and their exposure. Unlike existing studies that separate travel behavior modeling and emission estimation, the proposed approach integrates them within a unified framework, enabling exposure risk to actively influence path choice decisions.

2.2. Integration of environmental and health costs in dynamic path choice

In the context of static traffic assignment, the incorporation of environmental costs into travellers' decision-making is a well-established concept (2004). Al., 2003: Sun et al., 2018; Li et al., 2020; Luo et al., 2020). However, these studies often assume uniform cost sensitivity and overlook temporal dynamics and traveler heterogeneity. Recent research has extended this concept to dynamic contexts by incorporating emission costs into DTA models (Long et al., 2018; Pinto et al., 2020). This approach allows for a more accurate representation of temporal traffic fluctuations and their environmental impacts (Wang et al., 2018). These models suggest that pricing mechanisms can shift traffic away from emission-intensive routes toward more sustainable alternatives.

However, few studies consider both exposure and emission cost simultaneously. While some studies have explored traveler exposure as an externality (Pinto et al., 2020; Vosough et al., 2022), it is rarely internalised as a decision variable in route choice models. Moreover, most of the dynamic assignment models in this field remain confined to single-modal networks (Long et al., 2018; Tan et al., 2021). Although Pi et al. (2019) proposed a generalized formulation for multimodal DTA and

sought solutions for optimal travel costs, integrated models that account for mode choice, emissionand exposure-sensitive path selection, and cross-modal and multi-destination routing remain scarce.

This gap constrains the capacity to conduct comprehensive policy analyses on the trade-offs among
efficiency, emissions, and public health.

Overall, this study integrates both carbon emission and exposure costs into an extended multimodal DTA model. Theoretically, it enables the examination of how environmental and health factors jointly influence the dynamic distribution of traveler flow in a multimodal transport network. In practice, it captures the complete feedback loop between traffic flows and environmental health risks, enabling more refined evaluation of carbon pricing and public health interventions in multimodal networks.

3. Methodology

This section starts with introducing the emission model, which calculates the total emissions using a macroscopic emission model and captures the secondary health effects of carbon emissions through exposure using a Gaussian dispersion model. Next, to obtain the traffic flow inputs for the emission models, we adopt an extended multimodal DTA model, in which a generalized travel impedance function is introduced to account for both travel and emission exposure costs. Ultimately, the issue is expressed as a Variational Inequality (VI) and solved via an MSA algorithm.

3.1. Emission model

To effectively gauge the influence of vehicle emissions, we integrate a macroscopic emission framework with a Gaussian dispersion model. This approach allows us to quantify both the overall emission output and the subsequent health risks stemming from exposure to carbon pollutants.

3.1.1. Macroscopic emission model

This study adopts the macroscopic emission model proposed by Sharma and Mathew (2011), which defines the link-based carbon emission rate as a nonlinear relationship with link travel time. The same model has been applied in Heinold and Meisel (2020). In contrast to these studies, this study extends the model to a dynamic context, enabling it to calculate the evolution of emissions with temporal and spatial resolution. Mathematically, it is formulated as,

$$e_{m,a,t}^{n} = K_{m,1}^{n} \left(\frac{l_{a}}{\tau_{m,a,t}^{v}}\right)^{2} + K_{m,2}^{n} \left(\frac{l_{a}}{\tau_{m,a,t}^{v}}\right) + K_{m,3}^{n}, \forall n \in V, m \in M, a \in A, t \in T,$$
(1)

where $e_{m,a,t}^n$ represents the emission rate for link a in mode m, measured in grams per kilometer per vehicle (g/km/veh); $\tau_{m,a,t}^{v}$ denotes the travel time of link a in hours (h); and l_a is the length of link a in kilometer (km). $K_{m,1}^n, K_{m,2}^n$, and $K_{m,3}^n$ represent emission coefficients for various vehicle categories, determined through experimental analysis.

Using the link emission rate, the path's total emissions are determined by,

$$E_{m,p,t}^{w} = \sum_{a \in A} \sum_{n \in V} \Delta_{p}^{a,m,n} f_{m,a,t}^{n} e_{m,a,t}^{n} I_{a}, \forall w \in W, m \in M, p \in R_{m}^{w}, t \in T,$$
(2)

where $E_{m,p,t}^w$ denotes the carbon emission in grams associated with path p of mode m connecting OD pair w at time t (g). In the path-link incidence matrix, the element $\Delta_p^{a,m,n}$ is assigned a value of 1 if path p passes through link a and is represented by 0 in other cases. Meanwhile, $f_{m,a,t}^n$ represents the volume of traffic, measured in vehicles, moving along link a for mode m at a specific time t. Additionally, l_a denotes the length of link a, expressed in kilometers. This study then further converts the total amount of emissions to a monetary value $c_{m,e,p,t}^w$ using the unit carbon pricing approved by the European Union, which is \$48 (ECEEE, 2022).

3.1.2. Gaussian dispersion model and exposure estimation

Dispersion models describe pollutant dispersion from emission sources. Consistent with the

literature (Fallah-Shorshani et al., 2017; Mei and Liu, 2023), this study employs the widely used Gaussian dispersion model (Turner, 1994) expressed by,

$$c(x, y, z) = \frac{Q}{2\pi\sigma_y\sigma_z u} \exp\left(-\frac{y^2}{2\sigma_y^2}\right) \left[\exp\left(-\frac{(z-H)^2}{2\sigma_z^2}\right) + \exp\left(-\frac{(z+H)^2}{2\sigma_z^2}\right)\right]. \tag{3}$$

The concentration of emissions, denoted as c(x, y, z) in mg/m³, is measured at a receptor positioned at coordinates (x, y, z) within a localized coordinate framework. Here, Q stands for the emission rate of a point source, expressed in mg/s, while u represents the mean wind speed in meters per second. The height of the source is given by H in meters, and σ_y and σ_z correspond to the horizontal and vertical plume dispersion metrics, respectively, also in meters.

Drawing on the Gaussian dispersion framework, we expanded our analysis to assess how vehicle emissions spread along roadways, employing the approach developed by Benson (1984), which adapts the point-source dispersion model to accommodate line sources. Essentially, the method breaks down a road segment into several smaller sections, each representing an equivalent finite line source (FLS) with a specific emission rate, $Q_{\rm FLS}$, measured in mg/m/s. These FLS units are oriented perpendicular to the wind direction and centered at the midpoint of their respective segments. Since the x-axis aligns with the wind direction, all points on a given FLS share identical σ_y and σ_z values. Consequently, the concentration of emissions at a specific location (x,y,z), denoted as $c_{\rm FLS}(x,y,z=0)$, can be determined for each equivalent FLS.

$$c_{\text{FLS}}(x, y, z = 0) = \int_{y_{\text{FLS}}}^{\Delta} c(x, y, z = 0) dy = \frac{Q}{\pi \sigma_{y} \sigma_{z} u \sin \varphi_{\text{FLS}}} \int_{y_{\text{FLS}}}^{y_{\text{FLS}}^{2}} \exp \left(-\frac{y^{2}}{2\sigma_{y}^{2}}\right) dy, \tag{4}$$

where $y_{\rm FLS}^1$ and $y_{\rm FLS}^2$ represent the distances from the FLS endpoints to the x-coordinate; $\varphi_{\rm FLS}$ denotes the angle between the segment and the wind vector (°), $0^{\circ} \le \varphi_{\rm FLS} \le 90^{\circ}$.

Fig. 1 illustrates the conceptual process from vehicle emissions to the final estimation of exposure. Emissions from traffic activities are first dispersed using the Gaussian model to form a spatial concentration field. The detailed derivations of the emission dispersion and exposure concentration estimation process are provided in Appendix B. Based on this field, the travelers' exposure is calculated by integrating emission concentration over travel time and spatial extent.

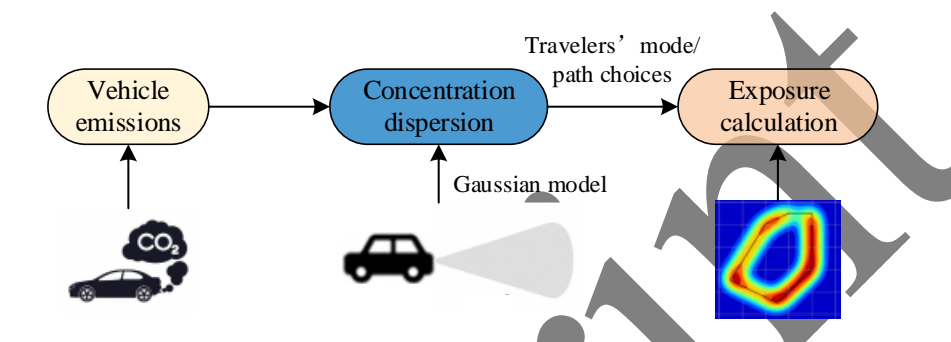


Fig. 1. Carbon emission dispersion and exposure estimation process.

The exposure concentration of travelers on link a is solely dependent on emissions from that link. The travelers' exposure concentration on link a at time t (mg·s/m³), $\mathcal{G}_{m,a,t}$, can be expressed as,

$$\mathcal{G}_{m,a,t} = \frac{\tau_a}{|l_a|} \sum_{n} \sum_{s \in F_a} C_{\text{FLS}}(x_s, y_s) = \frac{\tau_a}{|l_a|} \sum_{n} \sum_{s \in F_a} \frac{\sqrt{2} Q_{m,\text{FLS},t}^n}{\sqrt{\pi} \sigma_z u \sin \varphi_{\text{FLS}}} \left(\phi \left(\frac{y_{\text{FLS}}^2}{\sigma_y} \right) - \phi \left(\frac{y_{\text{FLS}}^1}{\sigma_y} \right) \right), \tag{5}$$

where t_a denotes the link travel time in hours (h); F_a is the FLS set on link a; $C_{FLS}(x_s, y_s)$ is the emission concentration at the center of the FLS; y_{FLS}^1 and y_{FLS}^2 are the distances from the measurement point (x_s, y_s) to the ends of FLS (m), respectively; $Q_{m,FLS,t}^n$ represents the line source emission rate at time t (mg/m/s), and the meanings of the other parameters are the same as those above.

The dispersion of each path can be obtained by summing the dispersion of the links included (Eq. (6)). The dispersion for each link is calculated as the product of dispersion concentration and traffic

volume, divided by travel time. Consequently, the exposure associated with path p at time t, $P_{m,p,t}^{w}$, equals the total exposure of type n across all links a along the path (mg), which is expressed by,

$$P_{m,p,t}^{w} = \sum_{a \in A} \sum_{n \in V} \Delta_{p}^{a,m,n} \frac{\mathcal{G}_{m,a,t}^{n} V_{m,a,t}^{n}}{3600 \tau_{a}} = \sum_{a \in A} \sum_{n \in V} \Delta_{p}^{a,m,n} \frac{\mathcal{G}_{m,a,t}^{n} l_{a} \omega_{t} h_{e}}{3.6 \tau_{a}}, \forall w \in W, m \in M, p \in R_{m}^{w}, t \in T,$$
(6)

where $V_{m,a,t}^n$ represents the dispersion volume of link a in mode m at time t, computed using $l_a \omega_l h_e$; l_a denotes the length of link a (in km), and W_l stands for the lane width (in m), with the assumption of $\omega_l = 3$; h_e is the dispersion height (m), assumed to be 1; τ_a denotes the link travel time in hours (h).

Then, the total exposures are converted into monetary value $c_{m,s,p,t}^{w}$. Since it is an indirect effect of emissions, the dispersion cost per ton is set at \$20, slightly lower than the cost of carbon emission.

3.2. Transportation model

We consider that passenger's mode and route choices are characterized by a nested logit model depicted in Fig. 2. In what follows, we define the cost associated with each travel mode, followed by the multimodal DTA model.

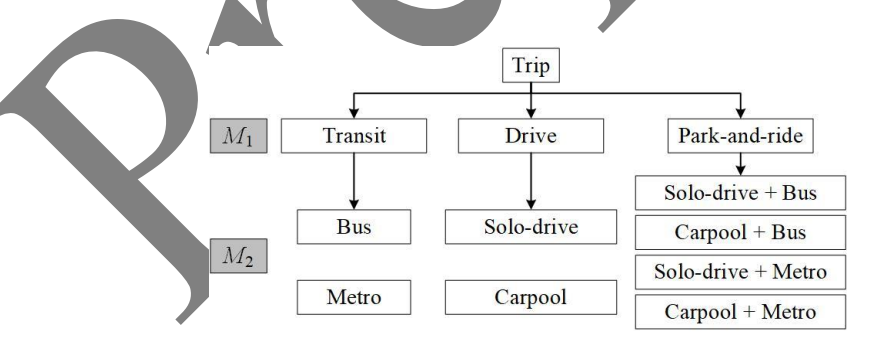


Fig. 2. The two-layer mode choices.

3.2.1. Generalized travel cost

Building on the research conducted by Pi et al. (2019), we establish a framework for calculating the generalized travel cost across various transportation options. The generalized travel cost, represented by $c_{m,p,t}^w$, $m \in \{\text{transit,drive,P\&R}\}$, is defined as the total expense incurred by a traveler

moving between OD pair w via travel mode m at departure time t along route p, $\forall p \in R_m^w$. Here, R_m^w stands for the collection of available paths for mode m between the specified OD pair.

$$c_{\text{transit},p,t}^{w} = \alpha g_{\text{transit},p,t}^{w} + \max[\beta(t + g_{\text{transit},p,t}^{w} - t^{*}), \gamma(t^{*} - t - g_{\text{transit},p,t}^{w})] + r_{p}^{w},$$

$$\forall p \in R_{m \in M_{2}(\text{Transit})}^{w}, w \in W, t \in T$$

$$(7)$$

$$c_{\text{drive},p,t}^{w} = \alpha g_{\text{drive},p,t}^{w} + \max[\beta(t + g_{\text{drive},p,t}^{w} - t^{*}), \gamma(t^{*} - t - g_{\text{drive},p,t}^{w})] + p_{i}/k + \Phi_{p,t}^{w}(k) + \theta,$$

$$\forall p \in R_{m \in M_{2}(\text{Car})}^{w}, w \in W, t \in T$$
(8)

$$c_{\text{P\&R},p,t}^{w} = \alpha g_{\text{P\&R},p,t}^{w} + \max[\beta(t + g_{\text{P\&R},p,t}^{w} - t^{*}), \gamma(t^{*} - t - g_{\text{P\&R},p,t}^{w})] + p_{i}/k + \Phi_{p,t}^{w}(k) + r_{p}^{w} + \theta,$$

$$\forall p \in R_{m \in M_{2}(\text{P\&R})}^{w}, w \in W, t \in T$$
(9)

where

- 1) $g_{m,p,t}^w$, $m \in \{\text{transit,drive,P\&R}\}$ represents the real travel time on path p at time t for OD pair w. The calculation for the paths corresponding to each mode is provided in Ap endix C.
- 2) t^* is the target time. α denotes the travel time unit cost. β and γ indicate the unit costs for early and late arrivals, respectively. The second term is called the schedule delay cost.
- 3) r_p^w denotes the fare for transit route p connecting OD pair w.
- 4) p_i represents the parking fee at slot i.
- 5) k denotes the total number of travelers sharing a ride, where k = 1 indicates a single driver traveling alone. Meanwhile, $\Phi_{p,t}^{od}(k)$ represents the carpool impedance cost on path p at time t for a trip between OD pair w with k passengers, $\Phi_{x,t}^{od}(1) = 0$.
- 6) θ as a measure of private car accessibility. If a traveler possesses a car or has the means to use one, θ is set to 0; otherwise, it is assigned to a large value to reflect the lack of access.
- 3.2.2. Generalized path impedance considering environmental cost

As calculated in Section 3.1 and Section 3.2.1, the factors to be considered in this study include the generalized travel cost, the carbon emission cost, and the traveler exposure cost. The total of the three is computed as the generalized impedance $\pi_{m,p,t}^{w}$ for path p between OD pair w at time t, as

in Eq. (10):

$$\pi_{m,p,t}^{w} = w_{1}c_{m,p,t}^{w} + w_{2}c_{m,e,p,t}^{w} + w_{3}c_{m,s,p,t}^{w}, \forall m \in M_{2}.$$

$$\tag{10}$$

We evaluate road network performance (total time, carbon emissions, and exposure) under three scenarios differentiated by path cost. The first scenario considers only generalised travel cost; the second incorporates emission costs; and the third further includes exposure costs.

3.2.3. Multimodal dynamic traffic assignment

All scenarios involve a nested logit model with two levels of mode choices. Let u(m) represent the second-layer mode options associated with the first-layer mode choice m. The two-layer condition of the extended multimodal DTA model can then be expressed as, $\forall w, t, m, u(m)$,

$$\begin{cases}
\pi_{m,u(m),p,t}^{w} \geq \mu_{m,u(m),t}^{w}, \forall p \in R_{m,u(m)}^{w}, f_{m,u(m),p,t}^{w} = 0, m \in M_{1}, u(m) \in M_{2} \\
\pi_{m,u(m),p,t}^{w} = \mu_{m,u(m),t}^{w}, \forall p \in R_{m,u(m)}^{w}, f_{m,u(m),p,t}^{w} > 0, m \in M_{1}, u(m) \in M_{2}
\end{cases}$$

$$\frac{d_{m,u(m),t}^{w}}{\sum d_{m,t}^{w}} = \frac{e^{-(a_{u(m)}^{m} + b_{2}^{m} \mu_{m,u(m),t}^{w})}}{\sum_{u' \in u(m)} e^{-(a_{u'}^{m} + b_{2}^{m} \mu_{m,u',t}^{w})}}, \forall m \in M_{1}, u(m) \in M_{2}$$

$$\mu_{m,t}^{w} = -\frac{1}{b_{2}^{m}} \ln \left(\sum_{u' \in u(m)} e^{-(a_{u'}^{m} + b_{2}^{m} \mu_{m,u',t}^{w})}\right), m \in \{\text{transit}, \text{drive}, P&R\}
\end{cases}$$
(11)

In the above equation, u(m) represents the set of all second-layer mode choices. $\mu_{m,u(m),t}^w$ is the equilibrium cost of travel mode m between OD pair w departing at time t. $f_{m,u(m),p,t}^w$ denotes the traffic flow along path p within mode m between OD pair w starting at time t. The flow of mode u(m) between OD pair w starting at time t is $d_{m,t}^w = \sum_{p \in R_{m,u(m),t}^w} f_{m,u(m),p,t}^w$. The total flow between OD pair w starting at time t is $q_t^w = \sum_{m \in \{\text{transit,drive},P\&R\}} d_{m,t}^w$. $a_{u(m)}^m$ and b_2^m serve as key parameters within the nested logit model.

It's worth noting that the last equation in Eq. (11) establishes the correlation between the first-layer and the second-layer modal equilibrium generalized impedance ($\mu_{m,t}^{w}$ and $\mu_{m,u(m),t}^{w}$). Finally, the modal flow between the OD pair w at each time t are:

$$d_{m,u(m),t}^{w} = \sum_{p \in R_{m,u(m),t}^{w}} f_{m,u(m),p,t}^{w}$$
(12)

$$d_{m,t}^{w} = \sum_{u(m)\in M_2} \sum_{p\in R_{m,u(m),t}^{w}} f_{m,u(m),p,t}^{w} = \sum_{u(m)\in M_2} d_{m,u(m),t}^{w}$$
(13)

It can be formulated as a VI problem $VI(\Lambda, \Omega_{m,u(m),p,t}^w)$, as demonstrated in \bigwedge 1 et al. (2019).

Find
$$\mathbf{f}^*$$
 such that $\Lambda(\mathbf{f}^*)^T \cdot (\mathbf{f} - \mathbf{f}^*) \ge 0, \ \forall \mathbf{f} \in \Omega_{m,u(m),p,t}^w$ (14)

where
$$\begin{cases} \Lambda(\mathbf{f}) = \left\{ \Lambda_{m,u(m),p,t}^{w}(\mathbf{f}) \right\} \\ \Lambda_{m,u(m),p,t}^{od}(\mathbf{f}) = \pi_{m,u(m),p,t}^{w}(\mathbf{f}) + \frac{a^{m} + \ln d_{m,t}^{w}}{b_{1}} + \frac{\ln d_{m,t}^{w}}{b_{2}^{m}} + \frac{a_{u(m)}^{m} + \ln d_{m,u(m),t}^{w}}{b_{2}^{m}} \end{cases}$$

$$\Omega_{m,u(m),p,t}^{w} = \left\{ \mathbf{f} \middle| \sum_{m} \sum_{u(m)} \sum_{p} f_{m,u(m),p,t}^{w} = q_{1}^{w} \right\}$$
(15)

Pi et al. (2019) remarked that the solution existence/uniqueness conditions of the classical multimodal DTA follow from VI theory. Proving its existence in the extended multimodal DTA framework is difficult due to model complexity. As this study does not address this proof, we assume that a VI solution exists. Since strict monotonicity on $\Omega_{m,u(m),p,t}^{w}$ is not universal, solutions may not be unique (**agurney, **09*). Although the existence of an extended multimodal DTA solution is not rigorously proven, the framework remains practical, as demonstrated by experiments showing that our solution method generally converges.

3.3. Solution method

3.3.1 Dynamic network loading

The DNL is a vital component in the DTA to assess the travel time in networks. It runs continuously during the designated study period, i.e., morning peak hours, in 5-second time intervals. The Cell Transmission Model (CTM) is employed to implement the DNL procedure. The algorithmic details within each time interval are detailed in Appendix D. Upon completion of the loading phase,

the model outputs travel times and traffic flows associated with each segment in the multimodal network. These results are then used to compute the generalized impedance for each origin-destination route, accounting for emissions from different vehicle categories and their associated exposure. Mode split, link/path flow, and travelers route choices are subsequently updated.

3.3.2 Method of Successive Averages

To solve the VI formulation of the extended multimodal DTA problem, this study employs the MSA algorithm for its simplicity and convergence performance. In our preliminary experiments, we compared MSA with another gradient projection method and found the latter performed worse. This is likely because the generalized path impedance is not monotonic, a property that is desirable for ensuring the convergence of gradient-based methods for solving VI problems. The main MSA iteration process is as follows. In essence, the algorithm iteratively averages the current solution with an auxiliary solution obtained by solving an auxiliary assignment problem (Kumar and Khani, 2023).

Step 1: Initialization. In a multimodal network, compute the shortest path between each OD based on the generalized path impedance $(\pi_{m,p,t}^w)$. Perform an all-or-nothing assignment for each OD pair to obtain the initial traffic flow of each link.

Step 2: Update the link flow matrix and generalized path impedance matrix. The weight to average the link flow between two consecutive iterations is set to be 1/(n+1). Then update path impedance matrix based on the averaged flow.

Step 3: Check convergence. If the following *Gap* satisfies the convergence accuracy, then terminate the algorithm; otherwise, return to step 2.

$$Gap = \frac{\sum_{w} \sum_{p \in R_{m,u(m),t}^{w}} \left(f_{m,u(m),p,t}^{w} \cdot \left(\pi_{m,u(m),p,t}^{w} - \min\left(\pi_{m,u(m),p,t}^{w} \right) \right) \right)}{\sum_{w} \sum_{p \in R_{m,u(m),t}^{w}} f_{m,u(m),p,t}^{w}}$$
(16)

3.3.3 Path set generation

The VI formulation requires knowing the set of paths. In the algorithm, we adopt the column

generation method to augment the path set at each iteration, and the algorithm is run to search for the shortest path across different modes. The overall algorithm for solving the extended multimodal DTA problem (11) is summarized in the algorithm in Appendix E.

4. Numerical results and discussion

We first solved the extended multimodal DTA problem on a simple testing network to assess the framework's efficiency and performance, and then conducted parameter sensitivity analyses to derive policy insights. The testing network in Section 4.1 is a simplified version of the multimodal network examined in Pi et al. (2019). Afterwards, we tested the model on a real-world multimodal network with multiple OD pairs, corresponding to the Pittsburgh metropolitan area network used in Pi et al. (2019). To ensure consistency and realism, the parameter settings in the test network were adopted directly from related real-world network studies. As a result, both the structural settings and behavioral parameters align with the original empirical context, enhancing the relevance and validity of our results.

4.1 A testing network

The network, depicted in Fig. 1, is a testing network featuring a single OD pair (O₁, D₁) with a demand of 10,000 vehicles. The network comprises 6 nodes, 6 links, a parking lot, a bus route, and a metro route. Section 2.1 notes that all travelers possess or can access private vehicles. In this experiment, travelers can choose any available travel mode. Link parameters are detailed in Table 1, while all paths are shown in Table 2.

Additional experimental parameters are provided in Table 3 (Pi et al., 2019). It is important to note that the parameter values in the nested logit model are drawn from existing empirical results (Ma and Qian, 2015; Ma and Qian, 2018; Ma et al., 2019), which provided calibrated values based on stated preferences or simulations. The values were selected to reflect typical cost sensitivities and behavioral realism in numerical simulations. For example, higher a^3 reflects greater sensitivity to generalized

impedance in the park-and-ride mode, while uniform b_1 and b_2 values ensure balanced nesting effects.

The coefficients $K_{m,1}^n, K_{m,2}^n$, and $K_{m,3}^n$ used in this study were initially proposed by Sharma and Mathew (2011), as listed in Table 4, based on regression analysis of field emission measurements and speed-flow data for cars and buses. These coefficients have been widely adopted in macroscopic emission modeling due to their practicality and robustness. In our implementation, they are treated as vehicle-type-specific and are assumed constant across the network. We acknowledge that this simplification may limit the model's adaptability to different urban contexts. However, the model structure allows for straightforward replacement of these parameters with locally calibrated values. In future applications, localized calibration could be conducted using empirical data from roadside monitoring, portable emissions measurement systems, or region-specific driving-cycle studies.

The wind speed and solar radiation level are both set at 1 (Tan et al., 2021), and is intended to provide a baseline for comparative analysis across scenarios. Although actual wind speeds may vary, our focus is on relative exposure patterns rather than precise concentration calibration. Similarly, the wind direction is 60° (ENE). The program is coded in C++ for dynamic model loading, with the MSA implemented in Python to compute the equilibrium solution, and executed on a desktop featuring an Intel(R) Core (TM) CPU i7-12700 @ 2.10GHz.

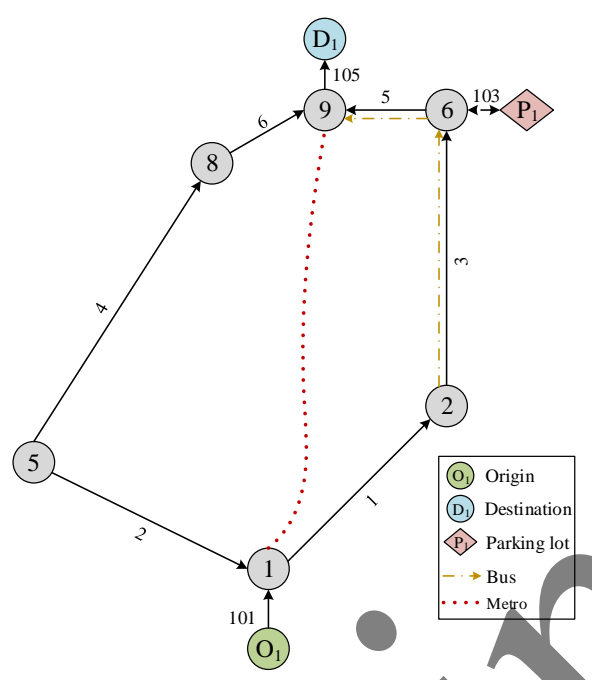


Fig. 3. A testing multimodal network.

Table 1Link parameters.

Link	Length (mile)	Lanes	v_1 (mile/	$c_1 \text{ (veh/h)}$	j_1 (veh/mile)	v ₂ (mile/h)	c_2 (veh/h)	j_2 (veh/mile)
l_1	5.0	2	40	2000	200	35	1200	100
l_2	7.5	3	65	2300	200	55	1200	100
l_3	3.5	2	40	2000	200	35	1200	100
l_4	4.0	3	65	2300	200	55	1200	100
l_5	1.5	2	40	2000	200	35	1200	100
l_6	1.5	3	65	2300	200	55	1200	100

Note: v denotes free-flow speed; c indicates lane capacity; j stands for jam density. Subscript 1 refers to cars, and subscript 2 refers to buses.

Table 2 All paths in the testing network.

Path	Mode	Sub-mode	Path
P_1	drive	solo-drive	$l_{101}, l_1, l_3, l_5, l_{105}$
P_2	drive	carpool	$l_{101}, l_2, l_4, l_6, l_{105}$
P_3	transit	metro	l_{101} , metro line, l_{105}
P_4	park&ride	drive+bus	$l_{101}, l_1, l_3, l_{103}, P_1, l_{103}, l_5, l_{105}$
P_5	transit	bus	$l_{101}, l_1, l_3, l_5, l_{105}$

Table 3 All other parameters.

Parameter	Value
Non-environmental cost model	$\alpha = 5.4$ \$/h $\beta = 2.8$ \$/h $\gamma = 16.6$ \$/h
Nested-logit model	$a^{1}, a^{1}_{u(1) \in U(1)} = 1.5$ $a^{2}, a^{2}_{u(2) \in U(2)} = 1.0$ $a^{3}, a^{3}_{u(3) \in U(3)} = 2.0$ $b_{1}, b_{2} = 1.0$
Parking slot	$w_{1,2} = 3$ \$/h $p_{1,2} = 1$ min $C_{1,2} = 20000$
Bus	$r_p^{w} = 2.75 waiting=8min frequency=20min
Metro	$r_p^w = 3.75 waiting=6min frequency=10min full trip=35min
Carpool	$\Phi_{p,t}^{w}(1) = 0$ $\Phi_{p,t}^{w}(2) = 1
Dynamic network loading	Starting/ending time=5AM/ 9AM intervals=2880 unit time=5s
Macroscopic emission model	$C_{co} = 48$ \$/t $C_{exposure} = 20$ \$/t
Gaussian dispersion model	$\varphi_e = 60^\circ$ $u = 1 \text{m/s}$

Table 4 Coefficients of emissions.

Vehicle type	K_1	K_2	K_3
Car	0.0020380	-0.22270	8.8100
Bus	0.0002483	-0.04090	1.698

4.1.1 Convergence result

We tested the extended multimodal DTA model within the network depicted in Fig. 3. Its solution algorithm was validated for performance and accuracy. The convergence of the equilibrium gap is plotted in Fig. 4.

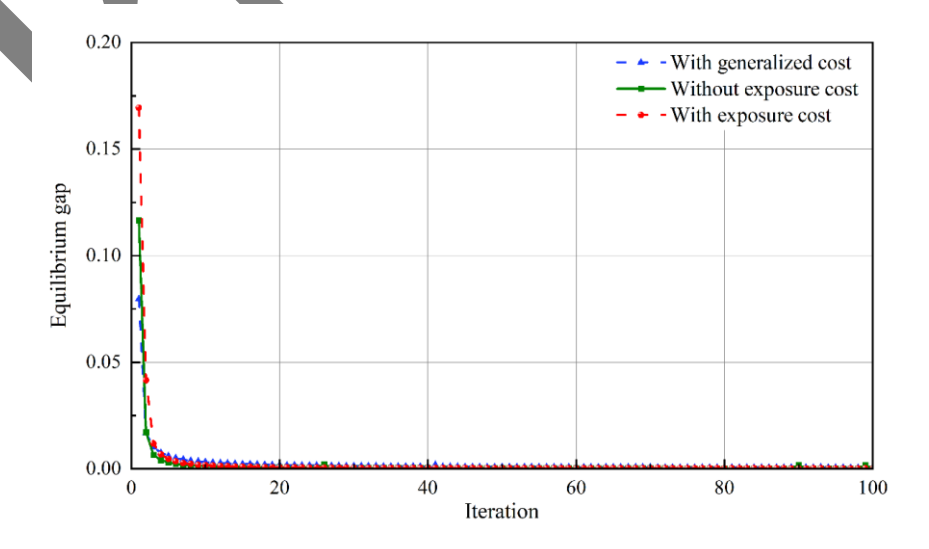


Fig. 4. Convergence curves for all scenarios in the testing network.

Table 5 Equilibrium results for all scenarios.

Scenario	Gap	Total	Total emission	Total	Total	Running
	value	time (h)	(kg)	exposure (kg)	cost (\$)	time (s)
Scenario 1	0.00046	343.0	28586.793	65909.641	7608.633	3619.91
Scenario 2	0.00014	341.6	19789.522	45626.676	8558.530	2551.77
Scenario 3	0.00019	336.4	15603.073	35974.409	9076.511	1858.10

Note: Scenarios 1, 2, and 3 represent "with generalized cost", "without exposure cost", and "with exposure cost", respectively. Total time denotes the aggregated travel time across all travelers. Total cost includes generalized travel costs, carbon emission costs, and exposure costs, depending on the scenario.

As shown in Fig. 4 and Table 5, all scenarios converge within 100 iterations. Incorporating carbon emission and exposure costs into the generalized cost framework reduces total travel time, emissions, and exposure compared to considering travel cost alone. Scenario 2 lowers emissions and exposure by 30.7% but increases total costs by 12.5%. Scenario 3 further reduces emissions and exposure by 45.4%, with a 2.0% decrease in travel time, albeit a 19.3% increase in total cost. These results suggest that while travel costs rise, scenario 3 offers the best trade-off between environmental and health benefits, representing the most sustainable solution among the three.

Contrary to the assumption that emission reduction increases travel time costs, scenario 3 shows a 2.0% decrease in total travel time (336.4 hours) compared to scenario 1 (343.0 hours). This reveals that travelers can choose shorter, less polluted routes without substantial time penalties. This suggests that environmental strategies may reduce both carbon emissions and exposure while improving travel efficiency, challenging the notion that such measures inherently increase time costs.

Table 5 also shows that when environmental factors are introduced for the first time (scenario 2), carbon emissions and exposure have significantly decreased (emissions by 8,797.3 kg, exposure by 20,282.96 kg), while costs have increased by \$949.90. However, when exposure is further reduced (scenario 3), the decrease in emissions and exposure becomes smaller, while the cost increases significantly (emissions decrease by 4,186.4 kg, exposure decreases by 9,649.27 kg, and costs rise by

\$517.98). According to Eqs. (7)-(9), generalized cost includes not only travel time but also schedule delay and transit fare, etc. Although total time decreases in scenario 3, the shift toward cleaner yet less direct travel modes, such as metro or bus, likely increases waiting, transfer, or walking time, thereby raising generalized cost. Additionally, minimizing exposure in congested areas often requires more dispersed traffic distributions, which can lead to system-level cost increases.

To better illustrate the trade-off, we introduce an indicative cost-benefit metric by comparing scenario 3 with scenario 1. The additional cost incurred per unit reduction in exposure is approximately \$0.049 per kg. This value reflects the economic input required to reduce a unit of exposure risk, and it can offer policymakers a quantitative reference when evaluating the health-economic efficiency of low-exposure strategies.

Nonetheless, as will be further demonstrated in the sensitivity analysis (Section 4.1.4), by appropriately adjusting the weights of emission and exposure costs, it is possible to achieve a simultaneous reduction in emissions, exposure, and total cost. This suggests that although scenario 3 shows the highest cost under current settings, adjusting these parameters could support more balanced outcomes, achieving health and environmental benefits without significantly increasing total cost compared to scenario 1.

In addition, we evaluated the computational performance of the proposed model. As shown in the final column of Table 5, the running times for scenarios 1 to 3 were 3619.91 seconds, 2551.77 seconds, and 1858.10 seconds, respectively. Interestingly, the inclusion of environmental cost factors (carbon emissions and exposure) not only improves environmental outcomes but also accelerates convergence by guiding the traffic redistribution more effectively.

4.1.2 Passenger flow distribution under three scenarios

Table 6 illustrates passenger flow distribution across five paths under three scenarios. Column 3 reflects the baseline scenario's initial traffic flow, while columns 4 to 6 show optimal assignments for scenarios in Table 5. Flow distribution shifts across scenarios: when generalized cost alone is considered, most travelers choose path 2 (carpool). However, with environmental factors included, at least 32.99% prefer path 4 (metro), followed by buses, likely influenced by road carbon emissions. Transit modes (metro and buses) offer the greatest environmental benefits, suggesting policymakers adjust metro routes to enhance commuting efficiency.

Table 6 Equilibrium passenger flow for 5 paths.

Path	Sub-mode	Initial	With generalized cost	Passenger flow Without exposure cost	With exposure cost
P_1	solo-drive	2000	1654	1388	1135
P_2	carpool	2000	3722	2131	1587
P_3	metro	2000	2248	3299	3777
P_4	drive+bus	2000	515	454	379
P_5	bus	2000	1861	2728	3122

4.1.3 Spatiotemporal carbon emission exposure

The spatiotemporal evolution of traveler exposure risk under different scenarios is illustrated in Fig. 5. Before 7 AM, exposure remains low and spatially scattered, despite isolated high-exposure spots. Between 7 AM and 8 AM, high-exposure areas become concentrated along major roads and bottlenecks, with values reaching their maximum. After 8 AM, exposure begins to decline, though some hotspots persist, suggesting a lag in concentration decay despite the dispersal of traffic flow.

In scenario 1, exposure is primarily concentrated near congested roads and intersections, indicating cumulative effects caused by bottlenecks. Introducing carbon emission costs (scenario 2) and especially exposure costs (scenario 3) leads to a more dispersed spatial pattern and lower peak values. This demonstrates that incorporating environmental costs into route choice effectively redistributes traffic and mitigates exposure concentration.

Notably, scenario 3 shows a substantial drop in peak exposure, highlighting the potential of

exposure costs to reduce localized health risks during peak periods. These findings underscore the importance of selecting paths that consider travel time, emissions, and exposure. Policymakers may consider integrating real-time monitoring, dynamic routing, and air quality alerts to reduce exposure risks while improving system-wide efficiency.

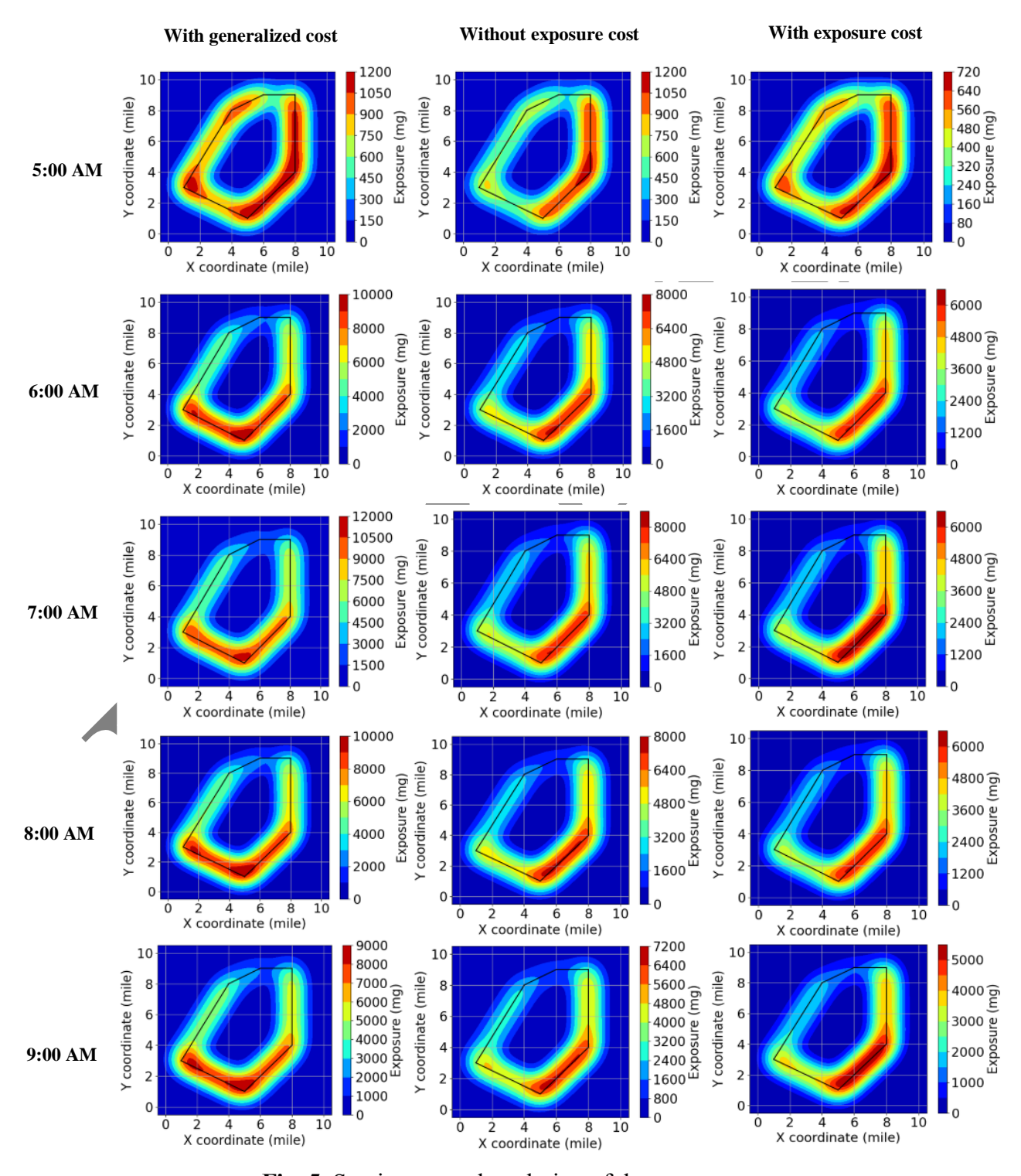


Fig. 5. Spatiotemporal evolution of the exposure.

When only generalized cost is considered, the distribution of high-exposure links is relatively concentrated, with distinct red peak areas, particularly in regions with dense core traffic flows. However, when both generalized cost and carbon emission cost are considered, the exposure peaks of high-exposure links decrease, and the spatial distribution of exposure shows a certain degree of diffusion. This occurs because the incorporation of carbon emission cost into route choice factors effectively redistributes traffic flow from certain high-exposure links. When generalized cost, carbon emission cost, and exposure cost are considered simultaneously, the peaks of high-exposure links are further reduced, and the exposure distribution becomes more uniform, with high-exposure areas (red) significantly shrinking. The improvement in exposure risk is particularly evident during peak hours, effectively mitigating the problem of excessively high local exposure concentrations.

These findings provide further evidence of the importance of capturing temporal variation in exposure, which can be achieved through the use of integrated dynamic modeling frameworks. In contrast, traditional static models can only provide aggregated results and ignore such fine-grained temporal evolution patterns.

4.1.4 Sensitive analysis on emission and exposure cost

To further explore the trade-offs discussed in Section 4.1.1, we investigate a sensitivity analysis on the weights of emission and exposure costs separately. The sensitivity of carbon emission cost is analyzed by controlling the weights of the other two costs, keeping them unchanged, i.e., $w_1 = w_3 = 1$. Specifically, the carbon emission cost weights are set at $w_2 = 3$, $w_2 = 5$, and $w_2 = 7$. Similarly, the sensitivity analysis of exposure cost is conducted in the same manner. The sensitivity changes are plotted as shown in Fig. 6. As the weight of carbon emission cost (w_2) increases, the path choice prioritizes the reduction of carbon emissions, while effectively inhibiting the increase in exposure.

Consequently, the total cost is decreased. On the other hand, as the weight of exposure cost (w_3) gradually increases, the travel path becomes more inclined to reduce the exposure risk to travelers. The data reveals a notable decline in both exposure levels and carbon emissions, which directly contributes to a drop in overall expenses. These findings suggest that the dynamic adjustment of the weighting coefficients of carbon emission and exposure cost in transportation management can achieve the dual minimization of carbon emissions and exposure risk in different zones and time periods. This provides a scientific basis for environmental management and public health protection in transportation systems.

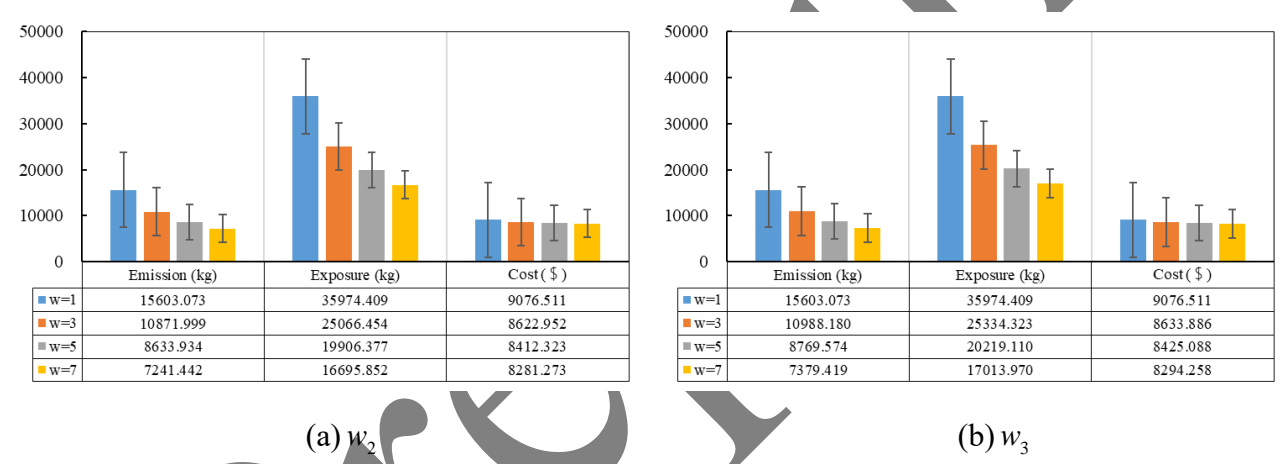


Fig. 6. The influence of changes in the weighting of carbon emissions and exposure costs.

The variations in carbon emissions, exposure, and total cost exhibit strong consistency as the weights of emission and exposure costs increase. This is likely due to the inherent causality: exposure risk arises primarily from vehicle emissions, leading to higher exposure costs, which in turn trigger changes in path choice. Incorporating both emission and exposure costs effectively penalizes high-emission links, guiding traffic flow toward lower-impact routes. Additionally, the reduction in carbon emissions and exposure is nonlinear for both w_2 and w_3 changes. While there is a decreasing trend with increasing coefficients, the marginal improvements diminish progressively.

An interesting observation is that although the increase in carbon emission and exposure cost

weights shows relatively similar effects in path choice, this does not mean that the two can be substituted for each other. Rather, it underscores the necessity of considering both in path choices. Specifically, considering only carbon emission costs may reduce environmental pollution but cannot fully address traveler exposure risks. Therefore, minimizing both emissions and exposure simultaneously remains challenging. These findings highlight the importance of jointly incorporating both cost components into path choice decisions to achieve a more balanced outcome between environmental and health benefits, as evidenced in Table 5.

Another key finding is that adjusting the weight of emission costs yields a more pronounced global effect in scenario 3, offering a stronger basis for system-level traffic management. This likely stems from the tendency of higher carbon cost weights to shift traffic away from high-emission links, which also tend to exhibit higher exposure levels, thus enabling a synergistic reduction in both emissions and exposure. Moreover, increasing emission cost weights may contribute to a more balanced traffic distribution, alleviating congestion on high-flow links and further reducing emissions and exposure per unit time. In contrast, increasing the weight of exposure costs effectively reduces localized exposure risks but does not target the root cause of emissions. As a result, its impact on system-wide emission control is limited. These findings suggest that unit carbon pricing functions not only as a climate policy but also as a critical public health strategy.

4.1.5 Sensitive analysis on wind speed and direction

We set the wind speed in the original model to five representative levels: Light air, Light breeze, Gentle breeze, Moderate breeze, and Fresh breeze (U.S. Naval Institute, 2024). All other parameters are held constant to analyze the effect of wind speed on travel equilibrium results. By solving the

multimodal dynamic traffic assignment problem under varying wind speed, Fig. 7 illustrates changes in total travel cost, CO₂ emissions, exposure levels, and route choice behaviors.

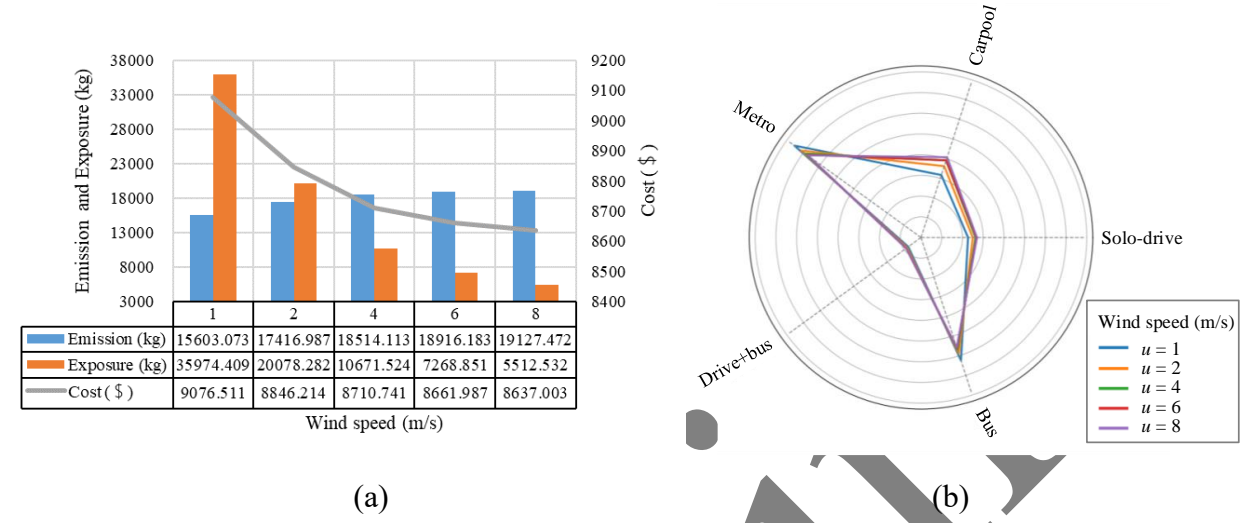


Fig. 7. (a) The influence of wind speed on emission, exposure, and travel cost. (b) Flow distributions under varying wind speed conditions.

The analysis results show that as wind speed increases, improved traffic flow slightly raises total emissions. However, enhanced atmospheric dispersion spreads emissions more quickly and reduces their concentration, leading to significantly lower exposure risks. Notably, total travel cost also declines as wind speed rises, suggesting a dual benefit of higher wind speeds on both mobility efficiency and health externalities. In addition, solo-driving and carpooling become more attractive under higher wind speeds, while the share of transit travelers, such as the metro and bus, declines. This suggests that in scenarios with high wind and better dispersion, health concerns are no longer a major reason for avoiding private car use, weakening the marginal health benefits of public transit. Therefore, neglecting dynamic meteorological factors in policymaking may lead to an underestimation of people's sensitivity to travel mode choices, undermining the effectiveness of green mobility promotion strategies.

We further set the wind direction angle to five representative values (60°, 90°, 150°, 240°, and 330°), while keeping all other parameters constant, to investigate how changes in wind direction affect

carbon exposure and route choice in the network. Fig. 8 presents the total travel cost, total emissions, exposure levels, and the resulting equilibrium traveler distributions under different wind directions.

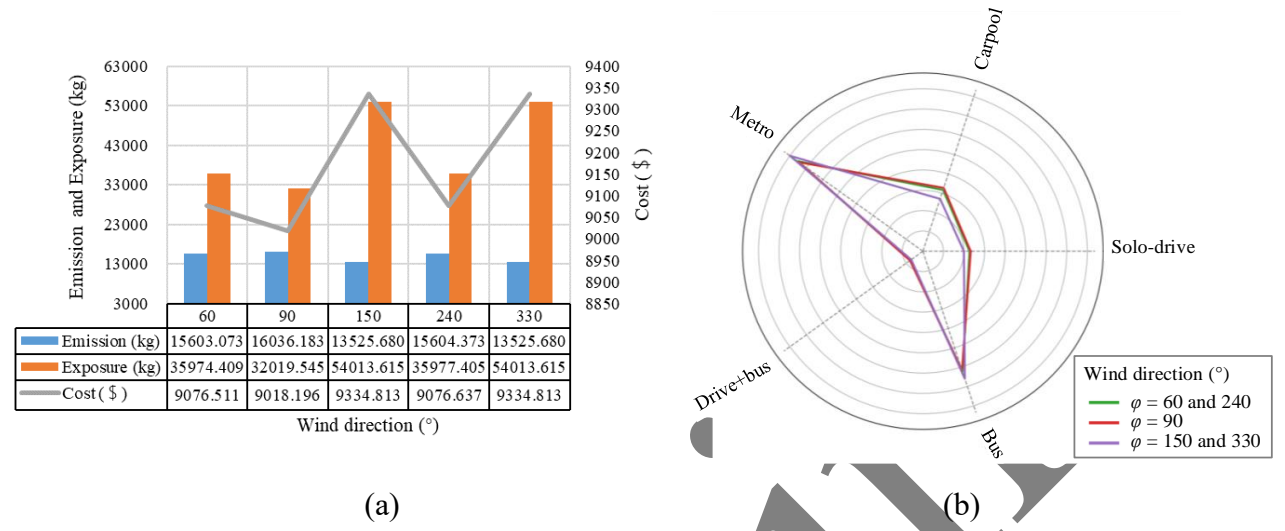


Fig. 8. (a) The influence of wind direction on emission, exposure, and travel cost. (b) Flow distributions under varying wind direction conditions.

The results reveal that spatial dispersion differences caused by wind direction lead to distinct exposure patterns. Both exposure and total cost exhibit periodic fluctuations, showing a consistent trend, indicating that wind direction indirectly affects cost. Overall, 90° and 150° correspond to the lowest and highest exposure levels, respectively, accompanied by shifts in the attractiveness of public transit. Interestingly, under 90°, although the exposure is the lowest, public transit becomes less attractive, while private driving increases. This counterintuitive outcome may be due to a shift in dispersion pathways: the new wind direction places bus corridors downwind, increasing their exposure intensity and thus their travel cost. In contrast, private cars, due to their greater routing flexibility, can more easily avoid high-exposure areas, making them relatively more appealing.

In addition, wind direction has a clearly symmetric effect on different travel modes. For example, the travel patterns under $\varphi = 60^{\circ}$ and $\varphi = 240^{\circ}$, as well as $\varphi = 150^{\circ}$ and $\varphi = 330^{\circ}$, are largely similar. This can be attributed to the functional symmetry of the Gaussian dispersion model with respect to wind direction, especially its dependence on $\sin \varphi_{\text{FLS}}$. This feature not only enhances our

understanding of the mechanism but also offers a pathway for optimizing future policy simulations. In the modeling process, selecting a representative subset of wind directions is sufficient to capture key trends, thereby maintaining accuracy while reducing computational load.

4.1.6 Sensitive analysis on new energy vehicle market penetration

We further examined how the penetration rate of new energy vehicles (NEVs) affects network performance. According to projections by the International Energy Agency, electric vehicles will account for over 25% of the global vehicle fleet by 2025 (IEA, 2025). To simulate this potential impact, we designed four market penetration scenarios - 10%, 15%, 20%, and 25% - while keeping all other parameters constant to solve the multimodal dynamic equilibrium problem. Here, NEVs refer only to zero-emission vehicles, such as battery electric vehicles and fuel cell vehicles. Fig. 9 illustrates total travel costs, emissions, exposure, and travel mode distributions under varying NEVs penetration levels.

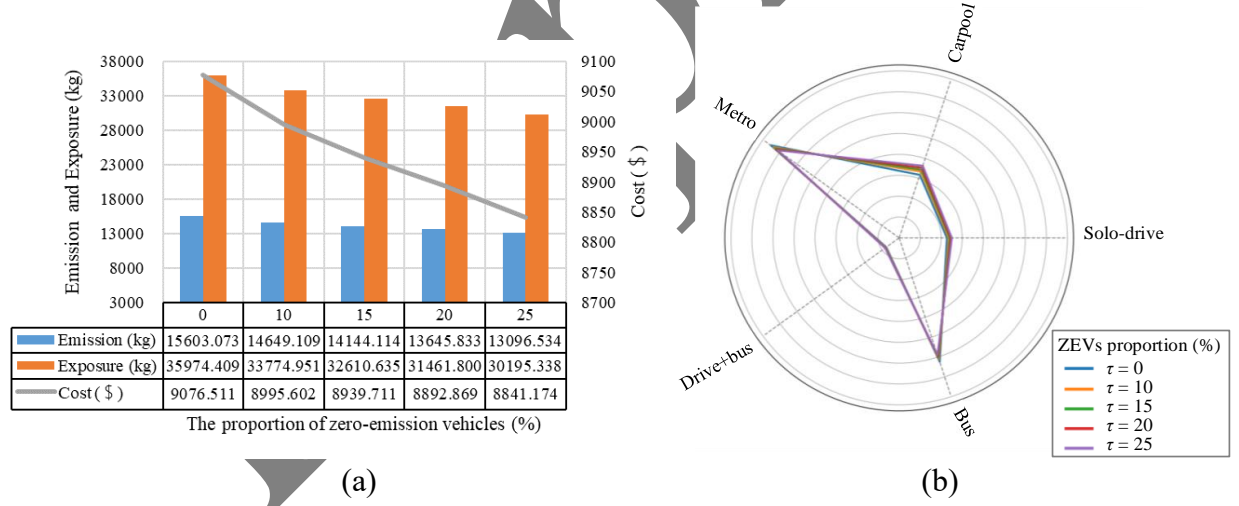


Fig. 9. (a) The influence of NEVs proportion on emission, exposure, and travel cost. (b) Flow distributions under varying NEVs proportion.

The results indicate that as the share of NEVs increases, both carbon emissions and health exposure risks significantly decrease, along with a consistent drop in total travel cost. Meanwhile, solo driving and carpooling have become more popular, while the share of public transit has slightly declined. This trend can be attributed to the zero tailpipe emissions of NEVs. Even with more travelers

choosing to drive, the overall exposure risk does not increase and may even drop. Additionally, the travel cost of NEVs is generally lower, especially when emission and exposure costs are integrated into the generalized path impedance $\pi_{m,p,t}^w$, making driving a more appealing option. This structural shift suggests that promoting NEVs not only supports emission reduction goals but also delivers both environmental and health benefits, without compromising accessibility or affordability. From a policy perspective, this reinforces the need to accelerate the replacement of conventional vehicles through subsidies, infrastructure improvements (e.g., charging networks), and emission control measures to foster a cleaner and more efficient urban transport system.

4.2 A simplified real-world network

To further evaluate the model's computational feasibility and applicability to real-world cases, we apply the framework to a multimodal urban network based on actual data from the Pittsburgh metropolitan area. The network consists of the I-79, PA 51, and US 19 highways, as well as a metro red line that connects the suburbs to downtown, as shown in Fig. 10(a). The simplified network is illustrated in Fig. 10(b). It comprises 4 origins (O₁ - O₄), 2 destinations (D₁ - D₂), 9 intersections, 16 road segments, three designated parking zones, a single bus route, and one metro line. The parking zones cover all available parking spaces in the area. The bus route stands in for all major high-frequency bus services, while the metro line represents the sole subway connection. This provides a substantially larger and more realistic setting than the testing network in Section 4.1.

The parameter values used in the real-world network are based on empirically calibrated data from prior studies (Ma and Qian, 2015; Ma and Qian, 2018; Ma et al., 2019), which incorporate local OD demand, road capacities, and fare structures from the Pittsburgh metropolitan area. During the morning peak (5 AM - 9 AM), the total passenger demand from origins O_1 - O_4 to destinations D_1 - D_2 is fixed

at 30,000. Notably, origins O_1 - O_4 represent large residential neighborhoods, while destinations D_1 - D_2 correspond to downtown Pittsburgh and the Mount Oliver residential area, respectively. These empirically grounded parameters serve as the basis for both the real-world network and the testing network introduced in Section 4.1. Table 7 provides the detailed link parameters, and Table 8 lists all feasible paths.

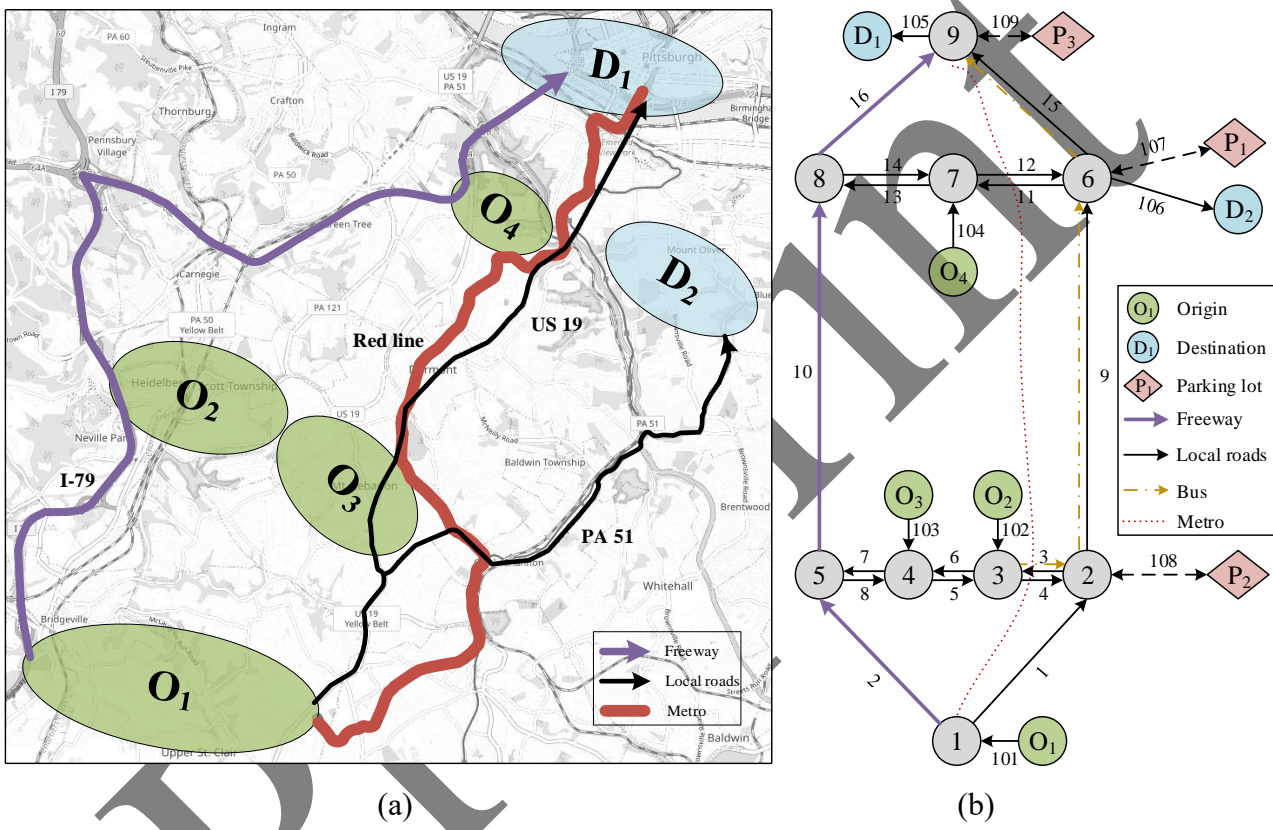


Fig. 10. (a) The actual network map shows that origins O_1 - O_4 are large residential areas. The two destinations are Downtown (D_1) and Mount Oliver (D_2). (b) A simplified multimodal network.

Table 7Link parameters.

Link	Length (mile)	Lanes	v_1 (mile/h)	c_1 (veh/h)	k_1 (veh/mile)	v_2 (mile/h)	c_2 (veh/h)	k_2 (veh/mile)
l_1	5	2	40	2000	200	35	1200	100
l_2	7.5	3	65	2300	200	55	1200	100
l_3	1.5	1	30	1800	200	25	1000	100
l_4	1.5	1	30	1800	200	25	1000	100
l_5	0.55	1	30	1800	200	25	1000	100
l_6	0.55	1	30	1800	200	25	1000	100
l_7	2.5	1	30	1800	200	25	1000	100

l_8	2.5	1	30	1800	200	25	1000	100	
l_9	3.5	2	40	2000	200	35	1200	100	
l_{10}	4	3	65	2300	200	55	1200	100	
l_{11}	0.5	1	30	1800	200	25	1000	100	
l_{12}	0.5	1	30	1800	200	25	1000	100	
l_{13}	0.5	1	30	1800	200	25	1000	100	
l_{14}	0.5	1	30	1800	200	25	1000	100	
l_{15}	1.5	2	40	2000	200	35	1200	100	
l_{16}	1.5	3	65	2300	200	55	1200	100	

Note: Same as Table 1.

Table 8List of paths.

Path	Origin	Destination	Mode	Sub-mode	Path
P_1	O ₁	D_1	drive	solo-drive	$l_{101}, l_2, l_{10}, l_{16}, l_{105}$
P_2			drive	solo-drive	$l_{101}, l_1, l_9, l_{15}, l_{105}$
P_3			drive	carpool	$l_{101}, l_2, l_{10}, l_{16}, l_{105}$
P_4			transit	metro	l_{101} , metro line, l_{105}
P_5			park&ride	drive+bus	l_{101} , l_1 , l_{108} , P_2 , l_{108} , l_9 , l_{15} , l_{105}
P_6			park&ride	drive+bus	l_{101} , l_2 , l_8 , l_5 , l_4 , l_{108} , P_2 , l_{108} , l_9 , l_{15} , l_{105}
P_7			park&ride	drive+bus	$l_{101}, l_1, l_9, l_{107}, P_1, l_{107}, l_{15}, l_{105}$
P_8			park&ride	drive+bus	l_{101} , l_2 , l_{10} , l_{14} , l_{12} , l_{107} , P_1 , l_{107} , l_{15} , l_{105}
P_9	O_3	D_1	drive	solo-drive	l_{103} , l_7 , l_{10} , l_{16} , l_{105}
P_{10}			drive	solo-drive	l_{103} , l_5 , l_4 , l_9 , l_{15} , l_{105}
P_{11}			drive	carpool	$I_{103}, l_7, l_{10}, l_{16}, l_{105}$
P_{12}			transit	bus	l ₁₀₃ , l ₅ , l ₄ , l ₉ , l ₁₅ , l ₁₀₅
P_{13}			park&ride	drive+bus	l_{103} , l_5 , l_4 , l_{108} , P_2 , l_{108} , l_9 , l_{15} , l_{105}
P_{14}	O ₄	D_1	drive	solo-drive	$l_{104}, l_{13}, l_{16}, l_{105}$
P_{15}			drive	solo-drive	$l_{104}, l_{12}, l_{15}, l_{105}$
P_{16}			drive	carpool	$l_{104}, l_{13}, l_{16}, l_{105}$
P_{17}	Ì	X .	park&ride	drive+bus	$l_{104}, l_{12}, l_{107}, P_1, l_{107}, l_{15}, l_{105}$
P_{18}	O_1	D_2	drive	solo-drive	$l_{101}, l_2, l_{10}, l_{14}, l_{12}, l_{106}$
P_{19}			drive	carpool	$l_{101}, l_1, l_9, l_{106}$
P_{20}			park&ride	drive+bus	l_{101} , l_2 , l_8 , l_5 , l_4 , l_{108} , P_2 , l_{108} , l_9 , l_{106}
P_{21}	O_3	D_2	drive	solo-drive	<i>l</i> ₁₀₃ , <i>l</i> ₅ , <i>l</i> ₄ , <i>l</i> ₉ , <i>l</i> ₁₀₆
P_{22}			drive	carpool	$l_{103}, l_7, l_{10}, l_{14}, l_{12}, l_{106}$
P_{23}			transit	bus	$l_{103}, l_5, l_4, l_9, l_{106}$

4.2.1 Convergence result

Fig. 11 demonstrates a good convergence and computational performance of the real-world network. Hence, this method holds promise for being applied to even more intricate, real transportation

networks down the line. Table 9 demonstrates that unit carbon pricing exerts a stronger moderating effect on carbon emissions and exposure in the real-world network. When considering generalized costs, emission costs, and exposure costs together, carbon emissions and exposure in the testing network (Section 4.1.1) decrease by 45%, whereas in the real-world network, they decrease by 78%. This is due to the increased presence of alternate routes in more complex networks, which provide travelers with increased flexibility to adapt, thereby reducing emissions and exposure more effectively. It can further be inferred that incorporating emission and exposure costs can generate more substantial environmental and health benefits in large cities or complex transportation networks. This has direct practical implications for policies such as green travel initiatives, low-emission zone planning, and public transport optimization in large cities.

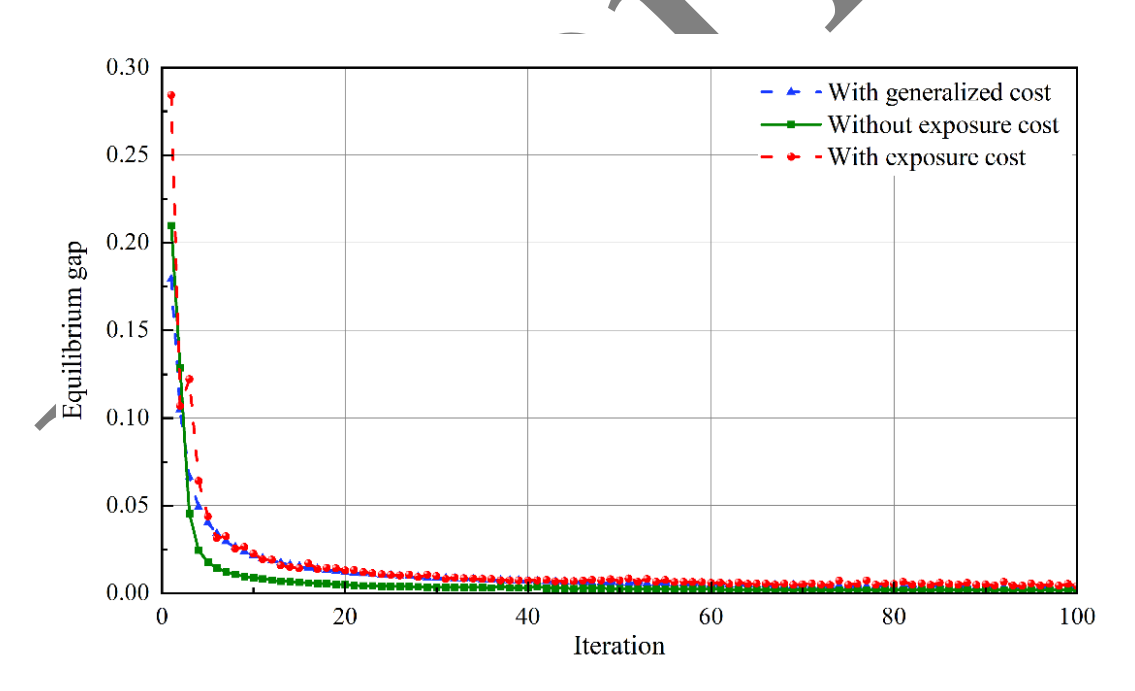


Fig. 11. Convergence curves for all scenarios in the Pittsburgh network.

Table 9 Equilibrium results for all scenarios.

Scenario	Gap	Total	Total	Total	Running
	value	time (h)	emission (kg)	exposure (kg)	time (s)
Scenario 1	0.00334	1300.902	413581.373	953552.230	4096.06
Scenario 2	0.00159	1295.397	214174.968	493801.297	3727.47
Scenario 3	0.00399	1280.884	88495.404	204034.793	3676.74

Note: Scenarios 1, 2, and 3 represent "with generalized cost", "without exposure cost", and "with exposure cost", respectively.

4.2.2 Passenger flow under three scenarios

Table 10 and Fig. 12 reveal that solo-drive in the slightly larger real-world network decreases significantly under scenario 3, whereas in the testing network, it remains at a certain level. This suggests that in such a real-world network, emission and exposure costs contributed to a reduction in solo driving. While this may reflect the influence of more diversified path options, further studies are required to assess whether similar patterns hold in other network settings. Additionally, in the testing network, the PnR model is nearly eliminated under Scenario 3. In contrast, in the slightly larger real-world network, the PnR model retains a certain number of travelers, although its growth trend is influenced by OD pair characteristics. This implies that PnR is not universally suitable for all travel demands, highlighting the need to incorporate OD pair characteristics into policymaking.

In summary, emission and exposure costs play a more significant role in promoting public transportation development. These findings can be reasonably extended to complex transportation networks. Furthermore, policy development should account for variations among different OD pairs. For instance, (O₁, D₁) exhibits the strongest public transportation substitution effect, suggesting that future efforts should prioritize enhancing public transit in this corridor. Similarly, (O₃, D₁) demonstrates a higher public transportation attraction, yet PnR remains a viable alternative for some travelers. This suggests that the planning of public transport routes should be an ongoing process.

Meanwhile, improving PnR facilities and enhancing transfer efficiency should be prioritized over simply increasing the unit carbon pricing.

Table 10 Equilibrium passenger flow for all paths.

Path		Cula mada	Passenger flow						
		Sub-mode	Initial	With generalized cost	Without exposure cost	With exposure cost			
	P_1	solo-drive	1250	1528	431	10			
	P_2	solo-drive	1250	1484	1112	16			
	P_3	carpool	1250	3226	904	12			
O_1 ,	P_4	metro	1250	2131	6217	9884			
\mathbf{D}_1	P_5	drive+bus	1250	512	695	52			
	P_6	drive+bus	1250	109	73	8			
	P_7	drive+bus	1250	514	407	10			
	P_8	drive+bus	1250	496	161	8			
	P_9	solo-drive	1200	923	547	82			
O ₃ ,	P_{10}	solo-drive	1200	790	654	84			
D_3 ,	P_{11}	carpool	1200	1948	1149	166			
D ₁	P_{12}	bus	1200	2103	3307	5240			
	P_{13}	drive+bus	1200	236	343	428			
	P_{14}	solo-drive	1250	1187	1157	979			
O ₄ ,	P_{15}	solo-drive	1250	1011	1072	1397			
D_1	P_{16}	carpool	1250	2507	2443	2065			
	P_{17}	drive+bus	1250	295	328	559			
O_1 ,	P_{18}	solo-drive	1667	2114	1115	613			
D_1 , D_2	P_{19}	carpool	1667	2798	3788	4165			
D ₂	P_{20}	drive+bus	1666	88	97	222			
O ₃ ,	P_{21}	solo-drive	1334	1798	1856	675			
D_3 ,	P_{22}	carpool	1333	1904	1577	866			
D ₂	P_{23}	bus	1333	298	567	2459			

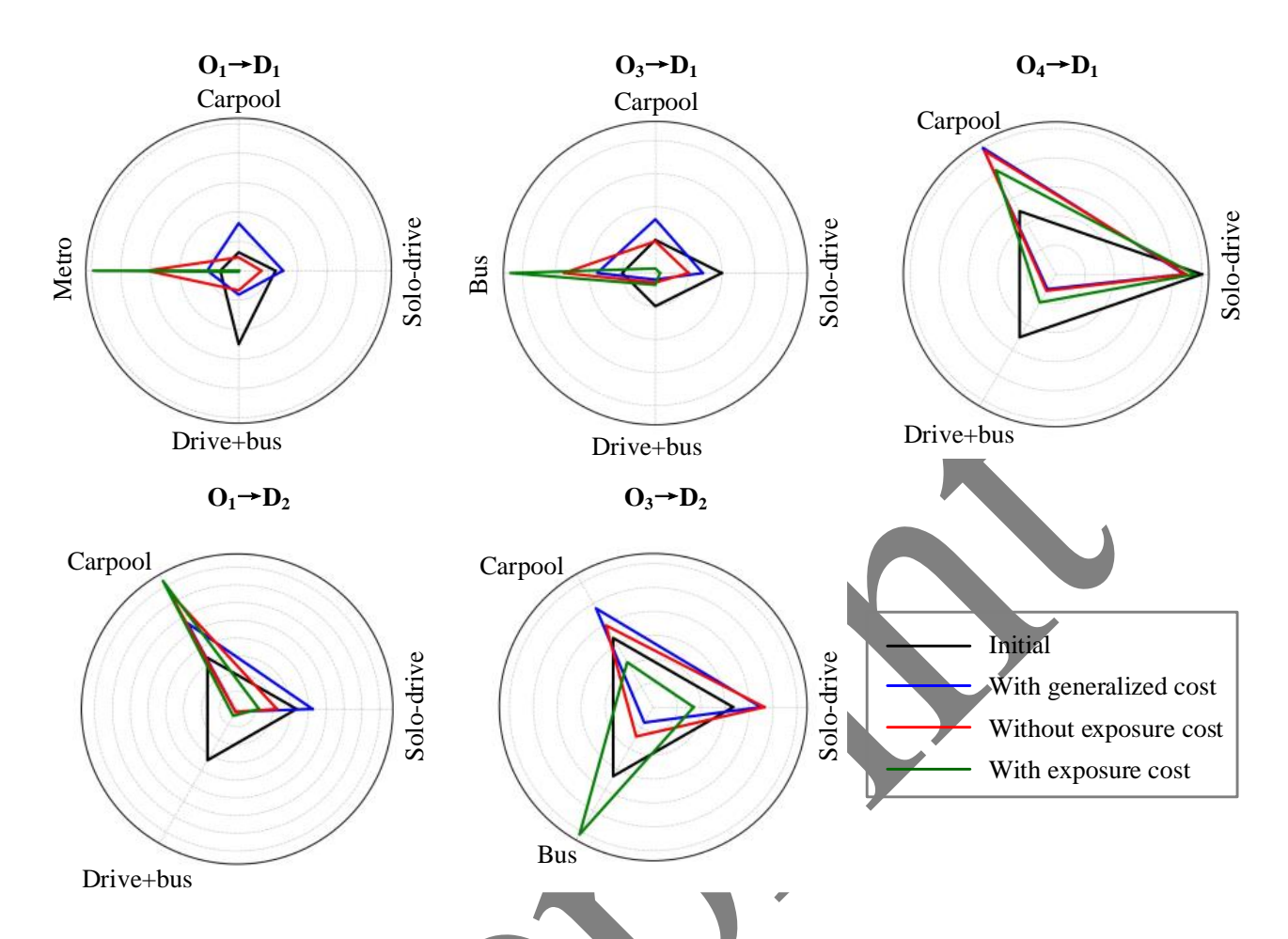


Fig. 12. Flow distribution under different scenarios.

4.3 Management policy implications

The examples above show that the integrated framework effectively facilitates a dynamically balanced distribution of traffic flows. This framework not only improves traffic efficiency but also serves as a scientific foundation for mitigating carbon emissions and exposure. While the numerical findings pertain to specific roadway systems and weather conditions, useful management perspectives can nevertheless be gained.

(1) The findings challenge the common assumption that environmental interventions inevitably increase travel time (Tan et al., 2021). In our scenarios, incorporating carbon and exposure costs into the path choice mechanism not only reduced emissions and exposure but also shortened total travel time. This indicates that appropriately calibrated environmental weights can improve overall network

performance by encouraging more efficient and equitable use of multimodal transportation resources.

- (2) The spatial evolution patterns reveal that high exposure zones tend to accumulate in bottleneck areas, even when total emissions are relatively low. To effectively manage exposure, traffic control strategies must incorporate both congestion and spatial dispersion effects, particularly near sensitive areas such as schools, hospitals, and elderly care facilities.
- (3) Emission and exposure costs promote modal shifts, but policy effectiveness varies across OD pairs. For example, the (O₁, D₁) corridor shows a strong substitution toward metro usage under considering environmental costs, while in (O₃, D₁), PnR remains a viable alternative. These differences highlight the need for tailored strategies. In some cases, improving transit frequency, enhancing transfer efficiency, and strengthening multimodal connections may yield greater benefits than further increasing environmental costs. Therefore, policy development should move beyond uniform pricing and adopt region-specific mixes of service upgrades, infrastructure investment, and behavioral incentives.
- (4) Compared with traditional models that consider only travel time or emissions, our framework demonstrates that incorporating exposure costs leads to a more balanced redistribution of traffic and mitigates local concentration peaks. This provides empirical support for incorporating exposure-based metrics into traffic assignment models and for extending the scope of carbon pricing mechanisms to include public health externalities.
- (5) Compared to increasing exposure cost weight, raising the emission cost weight leads to greater reductions in both emissions and exposure, while also lowering total cost. This advantage arises because emission costs influence path choice in a way that simultaneously avoids high emission and exposure links and promotes a more balanced spatial distribution of traffic flows. In contrast, exposure

costs primarily induce localized adjustments that do not directly reduce emissions at the source. From a policy perspective, this underscores the potential of unit carbon pricing not only as a climate instrument but also as an effective public health intervention.

4.4 Discussion of limitations

While the proposed framework demonstrates the feasibility of integrating dynamic traffic assignment with emission and exposure modeling in multimodal networks, it inevitably relies on several simplifying assumptions to ensure model tractability and computational efficiency. The following discussion identifies key assumptions and examines their implications for model accuracy and applicability in real-world scenarios.

- (1) The model assumes homogeneous traveler behavior, whereby all users respond to generalized travel costs, emission costs, and exposure costs in the same manner. Individual differences such as environmental preferences or habitual mode choices are not explicitly modeled. Although this assumption simplifies the behavioral structure and facilitates equilibrium computation, it may limit the model's ability to capture diverse traveler responses, particularly in policies involving eco-incentives or congestion pricing. Future extensions could incorporate behavioral heterogeneity through mixed logit or latent class models to improve realism.
- (2) The emission exposure component is modeled using a Gaussian dispersion framework, assuming steady meteorological conditions (e.g., constant wind speed and direction) and open-space road environments. This abstraction is common in the literature and enables efficient approximation of near-road pollutant concentrations (Tan et al., 2021). However, it may underestimate or misrepresent pollutant accumulation in urban street canyons, enclosed corridors, or under dynamic

atmospheric conditions. Incorporating time-varying meteorological inputs or more advanced dispersion models (e.g., RUNE or Computational Fluid Dynamics-based) would enhance accuracy in complex urban topographies (Mei and Liu, 2023; Gurram et al., 2019).

- (3) To ensure internal consistency and enable comparative analysis, both the transportation and emission models across the testing and real-world networks adopt the same parameter settings, derived from empirically calibrated studies (Ma et al., 2019; Sharma and Mathew, 2019). While this approach supports a unified modeling structure and focuses on evaluating the integrated framework, it may limit the predictive accuracy of specific case studies. Nonetheless, the framework allows for flexible adjustment of parameters using locally collected traffic counts, OD matrices, fare structures, and environmental data to support context-specific applications.
- (4) The road network representation and travel demand inputs are simplified to enable model testing and convergence analysis. Moreover, the model is solved using the MSA method, which, despite its simplicity and robustness, may exhibit slow convergence in large-scale or highly congested networks. Further improvements could include adaptive step-size adjustments or gradient-based solution methods to enhance scalability and efficiency.

5. Conclusions

This study proposes an integrated dynamic framework to improve travel time, carbon emissions, and exposure in a multimodal, multi-destination transportation network. The framework integrates a DTA model, an emissions model, and a dispersion model, providing a comprehensive lens to analyze the intricate interplay between diverse traffic patterns, parking, public transit operations, and shifts in transportation modes. Traveler decisions regarding mode and route selection are represented through a multi-layered nested logit model, while a VI approach is utilized to characterize the extended

multimodal DTA problem. Carbon emissions are estimated based on spatiotemporal passenger and vehicle flows and subsequently utilized to assess traveler exposure. The solution methodology employs an MSA to balance convergence and computational efficiency. To verify the model's effectiveness, numerical experiments are carried out on a testing network and a real-world multimodal transportation network. The results demonstrate that carbon emissions in a dynamic multimodal transportation network can be quantified, enabling an assessment of their impact on traveler health. Furthermore, considering only generalized costs (e.g., time, delay, and parking) in path selection may result in higher traveler exposure. In contrast, incorporating generalized travel cost, carbon emission cost, and exposure cost together achieves a balanced outcome, resulting in reductions in carbon emissions, exposure risks, and overall travel time. It is crucial to recognize that, although carbon emissions and exposure costs yield comparable outcomes, they emphasize different aspects of the system and thus neither should be considered in isolation.

The results emphasize the importance of adjusting route choices under dynamic traffic assignment in achieving the synergistic improvement of environmental sustainability, transportation efficiency, and public health. They offer foundational theories for designing and advancing eco-friendly smart transport networks. Moreover, the proposed extended multimodal DTA framework exhibits high flexibility and can be adapted to transportation systems across different spatial scales to inform planning and management decisions. Furthermore, this study highlights the substantial environmental benefits of public transportation. The extended multimodal DTA framework can serve as an indispensable resource for evaluating the effects of introducing new bus routes, optimizing stop locations, and integrating innovative public transportation options like microtransit and demand-responsive services (Xu et al., 2016, 2017), particularly concerning environmental and health

outcomes. Additionally, the framework can dynamically adjust operational strategies, including trip frequency, fleet size, and seating capacity, to enhance the overall effectiveness of public transportation systems (Jiang and Szeto, 2015). Finally, transportation management policies should incorporate differentiated measures based on the passenger flow characteristics of various OD pairs rather than relying solely on unit carbon pricing.

Our research has already identified several potential domains for further exploration. First, we plan to calibrate the model using daily multimodal traffic data and incorporate time-varying meteorological inputs (Shang and Zhang, 2013), thereby enhancing the model's accuracy and supporting more realistic and practical transportation management decisions. Furthermore, this study's findings provide a general framework for modeling and equilibrium assessment in extensive multidestination multimodal networks, which can encompass a wide range of travel modes, such as electric vehicles (Zhang et al., 2021), electric bases (Hu et al., 2025), ride-hailing (Wang et al., 2025), ridesharing, automated vehicles, etc (Slovet al., 2020, Zong and Yue, 2023). Last but not least, this research involves integrating personalized route selections for passengers, along with their cognitive levels and preferences (Jiang and Ceder, 2021), which may lead to equilibrium phenomena in stochastic traffic assignment.

CRediT authorship contribution statement

Yaxin Wu: Conceptualization, Methodology, Software, Validation, Formal analysis, Writing - original draft, Visualization, Writing - review & editing. Xiaowei Hu: Methodology, Writing - review & editing. Yujia Wang: Conceptualization, Methodology. Yu Jiang: Software, Writing - original draft, Writing - review & editing, Supervision.

Acknowledgements

This study was supported by the Fundamental Research Funds for the Central Universities (Grant No. HIT.OCEF.2022026), the National Natural Science Foundation of China (Grant No. 52272332, 52272308, 72574052), and the Heilongjiang Philosophy and Social Science Research Planning Project (Grant No. 24GLB006). The authors extend heartfelt thanks to Professor Jason (Xinyu) Cao for his profound expertise and unwavering support, which significantly contributed to the completion of this study.



Appendix A. Table of notations

The key notations are listed in Table A.1, while others are explained where they are used.

Table A.1 Key notations employed in this study.

Symbols	Description
w	index for OD pair
W	set of OD pairs
T	set of time intervals
$M_{_1}$	first-layer mode choices index
	$M_1 = \{\text{Transit, Driving, P&R}\}$
	second-layer mode choices index
M_2	$M_2(\text{Transit}) = \{\text{Bus, Metro}\}$
	$M_2(Driving) = \{Solo-driving, Carpooling\}$
	$M_2(P&R) = M_2(Driving) \times M_2(Transit)$
M	all mode choices index, $M = \bigcup_{i \in M_1} M_2(i)$
V	vehicle types, $V = \{car, bus, metro\}$
\mathbf{D}^{W}	set of paths of mode m connecting OD pair w.
R_m^w	$m \in M, w \in W$
A	set of links
	element is assigned a value of 1 if path p passes
$\Delta_p^{a,m,n}$	through link a and is represented by 0 in other
	cases

Appendix B. Derivation of exposure concentration estimation based on Gaussian dispersion

This appendix presents the detailed derivation of the exposure estimation procedure used in Section 3.1.2, including Gaussian dispersion model, FLS representation, and calculation of link exposure concentration.

B.1 Gaussian dispersion model for point sources

This study employs the widely used Gaussian dispersion model (Turne 1/94) expressed by,

$$c(x, y, z) = \frac{Q}{2\pi\sigma_y\sigma_z u} \exp\left(-\frac{y^2}{2\sigma_y^2}\right) \left[\exp\left(-\frac{(z-H)^2}{2\sigma_z^2}\right) + \exp\left(-\frac{(z+H)^2}{2\sigma_z^2}\right)\right]$$
(B.1)

The concentration of emissions, denoted as c(x, y, z) in mg/m³, is measured at a receptor positioned at coordinates (x, y, z) within a localized coordinate framework. Here, Q stands for the emission rate of a point source, expressed in mg/s, while u represents the mean wind speed in meters per second. The height of the source is given by H in meters, and σ_y and σ_z correspond to the horizontal and vertical plume dispersion metrics, respectively, also in meters. For urban settings, the values of σ_y and σ_z can be reasonably estimated using Eqs. (B.2) and (B.3) (Tan et al., 2021):

$$\sigma_y = 0.32x(1 + 0.0004x)^{-1/2}$$
, and (B.2)

$$\sigma_z = 0.24x(1+0.001x)^{-1/2}$$
 (B.3)

In examining vehicular emissions and concentrations at the local scale, we can designate z=0 and H=0. Then, Eq. (19.1) can be reformulated as

$$c(x, y, z = 0) = \begin{cases} \frac{Q}{\pi \sigma_y \sigma_z u} \exp\left(-\frac{y^2}{2\sigma_y^2}\right), & x \ge 0\\ 0, & x < 0 \end{cases}$$
(B.4)

where $x \ge 0$ and x < 0 differentiate the downwind and upwind direction, respectively.

B.2 Finite line source (FLS) representation

Drawing on the Gaussian dispersion framework, we expanded our analysis to assess how vehicle emissions spread along roadways, employing the approach introduced by Benson (1984). This technique adapts the point-source dispersion model to accommodate line sources. Essentially, the method breaks down a road segment into several smaller sections, each representing an equivalent FLS with a specific emission rate, $Q_{\rm FLS}$, measured in mg/m/s. These FLS units are oriented perpendicular to the wind direction, centered at the midpoint of their respective segments. Since the x-axis aligns with the wind direction, all points on a given FLS share identical σ_v and σ_z values. Consequently, the concentration of emissions at a specific location (x,y,z), denoted as $c_{\rm FLS}(x,y,z=0)$, can be determined for each equivalent FLS.

$$c_{\text{FLS}}(x, y, z = 0) = \int_{y_{\text{FLS}}}^{y_{\text{FLS}}^2} c(x, y, z = 0) dy = \frac{Q}{\pi \sigma_y \sigma_z u \sin \varphi_{\text{FLS}}} \int_{y_{\text{FLS}}}^{y_{\text{FLS}}^2} \exp\left(-\frac{y^2}{2\sigma_y^2}\right) dy,$$
 (B.5)

where y_{FLS}^1 and y_{FLS}^2 represent the distances from the FLS endpoints to the x-coordinate, computed using Eqs. (B.6) and (B.7):

$$y_{\text{FLS}}^{1} = y - \frac{l_{\text{FLS}} \sin \varphi_{\text{FLS}}}{2} \tag{B.6}$$

$$y_{\text{FLS}}^2 = y + \frac{l_{\text{FLS}} \sin \varphi_{\text{FLS}}}{2} \tag{B.7}$$

where $\varphi_{\rm FLS}$ indicates the angle relative to wind direction, $0^{\circ} \le \varphi_{\rm FLS} \le 90^{\circ}$; $l_{\rm FLS}$ represents the FLS's length. For more information, see Sun et al. (2018).

Eq. (B.5) can be further transformed by assuming that $r = y/\sigma_y$ and introducing $\phi(\cdot)$ to denote the standard normal distribution formula, which leads to,

$$c_{\text{FLS}}(x, y, z = 0) = \frac{Q}{\pi \sigma_z u \sin \varphi_{\text{FLS}}} \int_{\frac{J_{\text{FLS}}}{\sigma_y}}^{\frac{J_{\text{FLS}}}{\sigma_y}} \exp\left(-\frac{r^2}{2}\right) dr = \frac{\sqrt{2}Q}{\sqrt{\pi}\sigma_z u \sin \varphi_{\text{FLS}}} \left(\phi\left(\frac{y_{\text{FLS}}^2}{\sigma_y}\right) - \phi\left(\frac{y_{\text{FLS}}^1}{\sigma_y}\right)\right). \quad (B.8)$$

In the above equations, *Q* represents the emission rate of a point source. If we consider a FLS as a short link, then can be linked with the emission rate in the macroscopic emission model via the following equation,

$$Q_{m,\text{FLS},t}^{n} = e_{m,\text{FLS},t}^{n} \cdot f_{m,\text{FLS},t}^{n} \cdot \frac{v_{m,\text{FLS},t}^{n}}{3600l_{\text{FLS}}},$$
(B.9)

where $Q_{m,FLS,t}^n$ represents the line source emission rate at time t (mg/m/s), and $v_{m,FLS,t}^n$ represents the velocity of type n in FLS at time t (km/h).

B.3 Calculation of link exposure concentration

To calculate the emission exposure of a traveler while driving, we divide a link into a set of FLSs, and assume that there is a CO concentration measurement point s at the center of each FLS. Then, the exposure concentration of link a is computed by,

$$\mathcal{G}_a = \sum_{s \in F} C_{\text{FLS}}(x_s, y_s) \ t_s \,, \tag{B.10}$$

where F_a is the FLS set on link a; $C_{\text{FLS}}(x_s, y_s)$ is the emission concentration at the center of the FLS (Eq. (B.8)); (x_s, y_s) is the coordinate of the midpoint of a FLS on link a; t_s is the exposure duration within a FLS on link a, $\sum_{s \in F_a} t_s = \tau_a$; Assuming uniform travel time distribution on link a, $t_s = \tau_a/|l_a|$; $|l_a|$ represents the pre-determined count of finite line sources on link a.

Appendix C. Travel time calculation for each mode on the corresponding path

The travel time for every mode and route within the network is derived using the DNL model. For example, when driving, the total travel time encompasses the car trip from home to the parking lot, the time spent searching for a parking spot, and possibly the walk from the parking area to the final destination. For public transit, the calculation includes the walk from home to the bus stop, the waiting time for the bus or metro, the actual ride time, and the walk from the transit stop to the destination. In the case of PnR, the travel time factors in the car trip, the search for parking, the wait for the bus, the bus ride, and the walk from the bus stop to the destination. For further details on the calculations, readers are encouraged to consult Pi et al. (2019).

The metro system operates on a dedicated infrastructure, ensuring that travel times remain consistent with the schedule and are not disrupted by road traffic conditions. On the other hand, cars and buses share the same road networks, resulting in mixed traffic patterns. This study utilizes the DNL model to take into account the heterogeneous traffic propagation through links/nodes on the automobile network, which comprises light and heavy vehicles. To capture the complexities of heterogeneous traffic flow, we implement the multi-class traffic flow model developed by Qian et al. (2017). A key strength of this model lies in its ability to accurately represent queuing dynamics and spillback effects within the DNL framework. Additionally, the link model ensures a first-in-first-out (FIFO) principle for each vehicle class, allowing for precise calculation of travel times for cars and buses based on their respective cumulative flow curves.

The parking cruising time is generally anticipated to correlate with the expected parking availability in the designated area. A standard calculation for cruising time is expressed using

 $\frac{\varepsilon_i}{1-e_i(t)/C_i}$ (Qian and Rajagopal, 2014). Where ε_i signifies the average duration of a parking space

remains available when unoccupied. We denote the occupancy of parking zone i at time t as $e_i(t)$. C_i indicates the total capacity of the parking area. A widely recognized parking search time estimation model remains steady at low to moderate occupancy but rises sharply at high occupancy levels. For now, this DNL and the numerical example do not provide a simulation of street-side cruising for parking and its impacts on through traffic. However, the framework and solution algorithms concerning the extended multimodal DTA problem still apply to any generic dynamic simulation models.

This research utilizes the historical mean waiting time at each transit stop along the route, which is appropriate for high-frequency transit services during peak morning commute hours (Pi et al., 2018; Zhang and Qian, 2018). The time spent walking correlates directly with the distance walked. Assuming an individual's average walking speed is denoted as \overline{v} , the total time spent walking can be determined by simply dividing the distance by the average speed.

Appendix D. Dynamic network loading

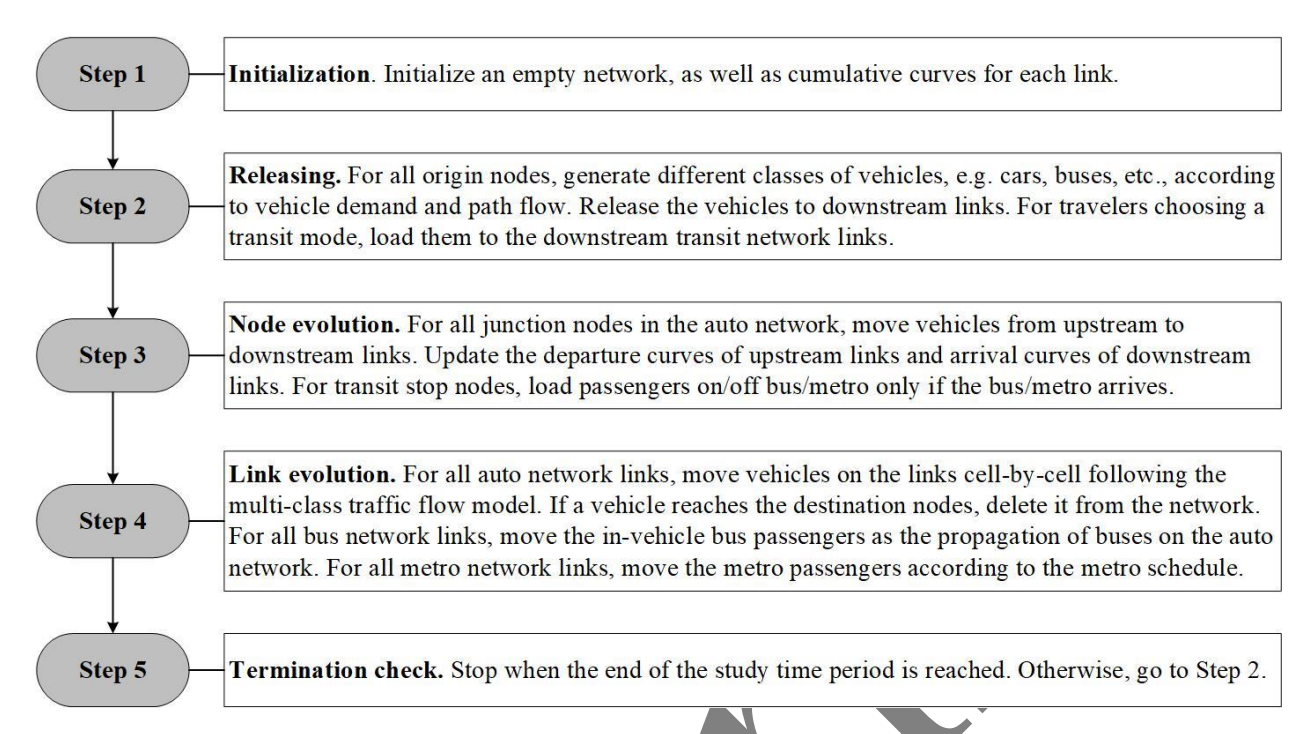


Fig. D.1. The dynamic network loading algorithm.



Appendix E. Algorithmetic steps for solving the extended multimodal DTA problem

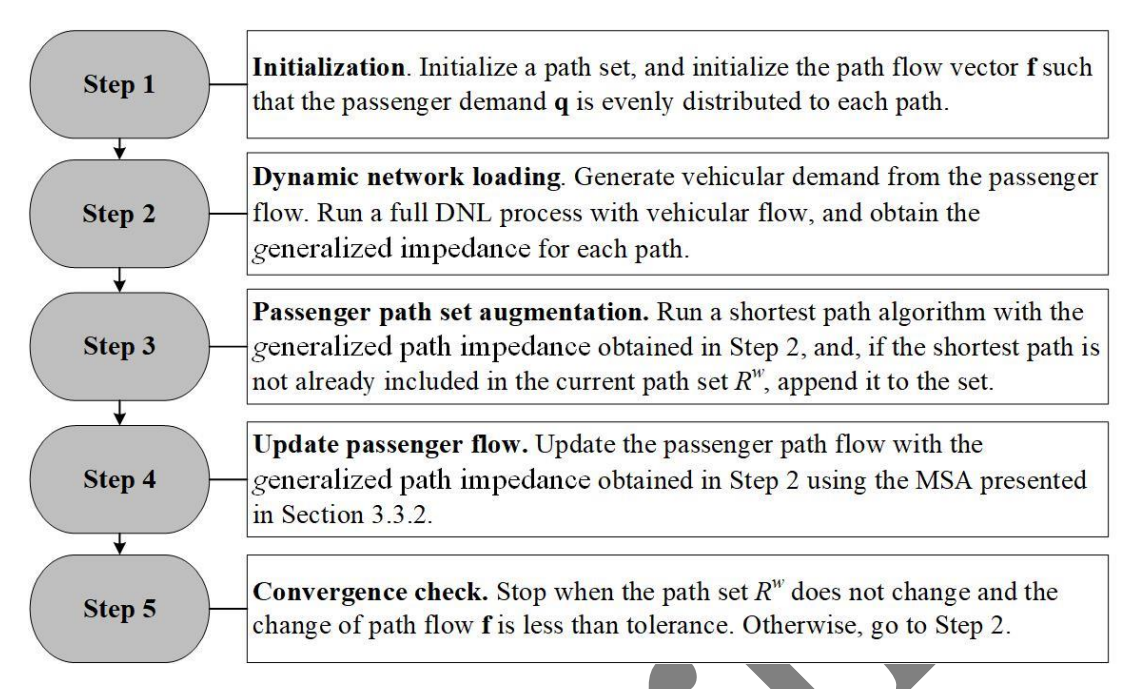


Fig. E.1. The algorithm of the extended multimodal DTA-Solver.



References

- Benson, P.E., 1984. CALINE4: A dispersion model for predicting air pollutant concentrations near roadways. Final Report, FHWA/CA/TL-84/15, Sacramento, CA. California Department of Transportation. https://searchworks.stanford.edu/view/2406352 [03.03.2025].
- Burns, J., Boogaard, H., Polus, S., Pfadenhauer, L.M., Rohwer, A.C., van Erp, A.M., Rehfuess, E.A., 2020. Interventions to reduce ambient air pollution and their effects on health: an abridged Cochrane systematic review. Environment International, 135, 105400.

 https://doi.org/10.1016/j.envint.2019.105400
- Dadashev, G., Levi, Y., Nahmias-Biran, B.H., 2023. Implications of de-carbonization policies using an innovative urban transport simulator. Transportation Research Part D: Transport and Environment, 119, 103754. https://doi.org/10.1016/j.tra.2023.103754
- Djavadian, S., Tu, R., Farooq, B., Hatzopoulou, M., 2020. Multi-objective eco-routing for dynamic control of connected & automated vehicles. Transportation Research Part D: Transport and Environment, 87, 102513. https://doi.org/10.1016/j.trd.2020.102513
- European Council for an Energy Efficient Economy (ECEEE), 2022. https://www.eceee.org/all-news/news/eu-approves-co2-tax-on-heating-and-transport-softened-by-new-social-climate-fund/ (Access: August 2024)
- Fallah-Shorshani, M., Shekarrizfard, M., Hatzopoulou, M., 2017. Integrating a street-canyon model with a regional Gaussian dispersion model for improved characterization of near-road air pollution. Atmospheric environment, 153, 21-31. https://doi.org/10.1016/j.atmosenv.2017.01.006
- Fan, Y.C., Ding, J.X., Long, J.C., Wu, J.J., 2024. Modeling and evaluating the travel behaviour in multimodal networks: A path-based unified equilibrium model and a tailored greedy solution

algorithm. Transportation Research Part A: Policy and Practice, 182, 104032. https://doi.org/10.1016/j.tra.2024.104032

- Gurram, S., Stuart, A.L., Pinjari, A.R., 2019. Agent-based modeling to estimate exposures to urban air pollution from transportation: Exposure disparities and impacts of high-resolution data.

 Computers Environment and Urban Systems, 75, 22-34.

 https://doi.org/10.1016/j.compenvurbsys.2019.01.002
- He, Z.B., Zhang, W.Y., Jia, N., 2020. Estimating carbon dioxide emissions of freeway traffic: A spatiotemporal cell-based model. IEEE Transactions on Intelligent Transportation Systems, 21(5), 1976-1986. https://doi.org/10.1109/TITS.2019.2909316
- Heinold, A., Meisel, F., 2020. Emission limits and emission allocation schemes in intermodal freight transportation. Transportation Research Part E: Logistics and Transportation Review, 141, 101963. https://doi.org/10.1016/j.tre.2020_101963
- Hu, X.W., Qiu, Z.Y., Gao, W., 2025. Optimization of electric bus dispatching interval considering stochastic traffic conditions. Transportation Letters-The International Journal of Transportation Research, 17(2), 200-213. https://doi.org/10.1080/19427867.2024.2335735
- International Energy Agency (IEA), 2025. Global EV Outlook 2025. https://www.iea.org/reports/global-ev-outlook-2025/executive-summary (Access: August 2025)
- Jia, T., Zhang, P.C., Chen, B.Y., 2022. A microscopic model of vehicle CO₂ emissions based on deep learning-- A spatiotemporal analysis of taxicabs in Wuhan, China. IEEE Transactions on Intelligent Transportation Systems, 23(10), 18446-18455.
 https://doi.org/10.1109/TITS.2022.3151655
- Jiang, Y., Szeto, W.Y., 2015. Time-dependent transportation network design that considers health

cost. Transportmetrica A: transport science, 11(1), 74-101. https://doi.org/10.1080/23249935.2014.927938

- Kamishetty, S., Vadlamannati, S., Paruchuri, P., 2020. Towards a better management of urban traffic pollution using a Pareto max flow approach. Transportation Research Part D: Transport and Environment, 79, 102194. https://doi.org/10.1016/j.trd.2019.11.023
- Kumar, P., Khani, A., 2023. Schedule-based transit assignment with online bus arrival information.

 Transportation Research Part C: Emerging Technologies, 155, 104282.

 https://doi.org/10.1016/j.trc.2023.104282
- Li, D., Yang, M., Jin, C., Ren, G., Liu, X., Liu, H., 2020. Multi-modal combined route choice modeling in the MaaS age considering generalized path overlapping problem. IEEE Transactions on Intelligent Transportation Systems, 22(4), 2430-2441.
 https://doi.org/10.1109/TITS.2020.3030707
- Liang, M.Z., Chao, Y., Tu, Y., Xu, T., 2023. Vehicle pollutant dispersion in the urban atmospheric environment: A review of mechanism, modeling, and application. Atmosphere, 14(2), 279. https://opi.org/10.3390/atmos/4020279
- Long, J., Chen, J., Szeto, W.Y., Shi, Q., 2018. Link-based system optimum dynamic traffic assignment problems with environmental objectives. Transportation Research Part D: Transport and Environment, 60, 56-75. https://doi.org/10.1016/j.trd.2016.06.003
- Lu, H., Xiao, C.Y., Jiao, L.D., Du, X.S., Huang, A.Q., 2024. Spatial-temporal evolution analysis of the impact of smart transportation policies on urban carbon emissions. Sustainable Cities and Society, 101, 105177. https://doi.org/10.1016/j.scs.2024.105177
- Luo, J., Boriboonsomsin, K., Barth, M., 2020. Consideration of exposure to traffic-related air

pollution in bicycle route planning. Journal of Transport & Health, 16, 100792. https://doi.org/10.1016/j.jth.2019.100792

- Ma, W., Qian, S., 2015. Traffic impact of the greenfield bridge closure. The public works of pittsburgh technical report, Technical report. Civil and Environmental Engineering, Carnegie Mellon University.
- Ma, W., Qian, Z.S., 2018. Estimating multi-year 24/7 origin-destination demand using high-granular multi-source traffic data. Transportation Research Part C: Emerging Technologies, 96, 96-121. https://doi.org/10.1016/j.trc.2018.09.002
- Ma, W., Pi, X., Qian, S., 2019. Estimating multi-class dynamic origin-destination demand through a forward-backward algorithm on computational graphs. arXiv preprint arXiv: 1903.04681. https://doi.org/10.48550/arXiv.1903.04681
- Ma, R., Ban, X. (J.), Szeto, W. Y., 2017. Emission modeling and pricing on single-destination dynamic traffic networks. Transportation Research Part B: Methodological, 100, 255-283. https://doi.org/10.1016/j.trb.2017.02.007
- Mei, D., Liu, C., 2023. Bi-objective optimization of traffic assignment with air quality consideration via CFD-based surrogate model. Sustainable Cities and Society, 91, 104425.

 https://doi.org/10.1016/j.scs.2023.104425
- Mohsenizadeh, M., Tural, M.K., Kentel, E., 2020. Municipal solid waste management with cost minimization and emission control objectives: A case study of Ankara. Sustainable Cities and Society, 52, 101807. https://doi.org/10.1016/j.scs.2019.101807
- Nagurney, A., 2009. Variational inequalities. Encyclopedia of Optimization, pp. 3989-3994.
- Pi, X., Egge, M., Whitmore, J., Silbermann, A., Qian, Z.S., 2018. Understanding transit system

- performance using avl-apc data: an analytics platform with case studies for the Pittsburgh region.

 Journal of Public Transportation, 21(2), 19-40. https://doi.org/10.5038/2375-0901.21.2.2
- Pi, X., Ma, W., Qian, Z.S., 2019. A general formulation for multi-modal dynamic traffic assignment considering multi-class vehicles, public transit and parking. Transportation Research Part C: Emerging Technologies, 104, 369-389. https://doi.org/10.1016/j.trc.2019.05.011
- Pinto, J. A., Kumar, P., Alonso, M. F., Andreao, W. L., Pedruzzi, R., dos Santos, F. S., Moreira, D.M., Albuquerque, T.T., 2020. Traffic data in air quality modeling: a review of key variables, improvements in results, open problems and challenges in current research. Atmospheric Pollution Research, 11(3), 454-468. https://doi.org/10.1016/j.apr.2019.11.018
- Qian, Z.S., Li, J., Li, X., Zhang, M., Wang, H., 2017. Modeling heterogeneous traffic flow: a pragmatic approach. Transportation Research Part B: Methodological, 99, 183-204. https://doi.org/10.1016/j.trb.2017.01.011
- Qian, Z.S., Rajagopal, R., 2014. Optimal dynamic parking pricing for morning commute considering expected cruising time. Transportation Research Part C: Emerging Technologies, 48, 468-490. https://doi.org/10.1016/j.trc.2014.08.020
- Shang, B., Zhang, X.N., 2013. Study of travel mode choice behavior based on nested logit model.

 Applied Mechanics and Materials, 253-255, 1345-1350.

 https://doi.org/10.4028/www.scientific.net/AMM.253-255.1345
- Sharma, S., Mishra, S, 2011. Optimal emission pricing models for containing carbon footprints due to vehicular pollution in a city network. In: Proceedings of the 90th Transportation Research Board Annual Meeting, Washington, D.C. https://api.semanticscholar.org/CorpusID:107619636
- Sharma, S., Mathew, T.V., 2011. Multi-objective network design for emission and travel-time trade-

- off for a sustainable large urban transportation network. Environment and Planning B: Planning and Design, 38(3), 520-538. https://doi.org/10.1068/b37018
- Shen, L., Chen, Z., Dou, X., Xu, X., Cao, Z., Liao, S., 2024. Restricting factors for promoting electric vehicles: evidence from China. Transport Policy, 148, 234-245.

 https://doi.org/10.1016/j.tranpol.2024.01.017
- Shi, X.W., Yao, H.D., Liang, Z.H., Li, X.P., 2022. An empirical study on fuel consumption of commercial automated vehicles. Transportation Research Part D: Transport and Environment, 106, 103253. https://doi.org/10.1016/j.trd.2022.103253
- Song, Z.R., Zang, L.L., Zhu, W.X., 2020. Study on minimum emission control strategy on arterial road based on improved simulated annealing genetic algorithm. Physica A: Statistical Mechanics and its Applications, 537, 122691. https://doi.org/10.1016/j.physa.2019.122691
- Sun, Z., Tan, Y., Ma, R., Yang, X., Zhang, J., 2018. Multiple equilibrium behaviors considering human exposure to vehicular emissions. Journal of Advanced Transportation, 9365120, 1-10. https://doi.org/10.1156/2018/9365120
- Szeto, W.Y., Wong, S.C., 2012. Dynamic traffic assignment: model classifications and recent advances in travel choice principles. Central European Journal of Engineering, 2(1), 1-18. https://doi.org/10.2478/\$13531-011-0057-y
- Tan, Y., Ma, R., Sun, Z., Zhang, P., 2021. Emission exposure optimum for a single-destination dynamic traffic network. Transportation Research Part D: Transport and Environment, 94, 102817.
 https://doi.org/10.1016/j.trd.2021.102817
- Turner, D.B., 1994. Workbook of atmospheric dispersion estimates: an introduction to dispersion modeling. 2nd Ed. CRC Press, London. https://doi.org/10.1201/9780138733704

- U.S. Naval Institute, 2024. The origins of the Beaufort scale. https://www.usni.org/magazines/naval-history-magazine/2024/march/origins-beaufort-scale (Access: August 2025)
- Vosough, S., de Palma, A., Lindsey, R., 2022. Pricing vehicle emissions and congestion externalities using a dynamic traffic network simulator. Transportation Research Part A: Policy and Practice, 161, 1-24. https://doi.org/10.1016/j.tra.2022.04.017
- Wang, H., Hu, X.W., Zhang, Y.T., An, S., 2025. Analysis of ride-hailing service discontinuity: Links to built environment and public transportation. Journal of Transport Geography, 126, 104242. https://doi.org/10.1016/j.jtrangeo.2025.104242
- Wang, Y., Szeto, W.Y., Han, K., Friesz, T.L., 2018. Dynamic traffic assignment: A review of the methodological advances for environmentally sustainable road transportation applications.
 Transportation Research Part B: Methodological, 111, 370-394.
 https://doi.org/10.1016/j.trb.2018.03.011
- Xi, H.N., Shao, Z.Q., Hensher, D.A., Nelson, J.D., Chen, H.M., Wijayaratna, K., 2025. A multi-task Transformer with mixture-of-experts for personalized periodic predictions of individual travel behavior in multimodal public transport. Transportation Research Part C: Emerging Technologies, 179, 105287. https://doi.org/10.1016/j.trc.2025.105287
- Xu, S., Zhang, L., Zhang, P., Noh, H.Y., 2016. An indirect traffic monitoring approach using building vibration sensing system. In: Proceedings of the 14th ACM Conference on Embedded Network Sensor Systems CD-ROM. ACM, pp. 374-375. https://doi.org/10.1145/2994551.299671
- Xu, S., Zhang, L., Zhang, P., Noh, H.Y., 2017. An information-theoretic approach for indirect train traffic monitoring using building vibration. Frontiers in Built Environment, 3, 22.

 https://doi.org/10.3389/fbuil.2017.00022

- Zeng, W., Miwa, T., Morikawa, T., 2020. Eco-routing problem considering fuel consumption and probabilistic travel time budget. Transportation Research Part D: Transport and Environment, 78, 102219. https://doi.org/10.1016/j.trd.2019.102219
- Zhang, P., Qian, Z.S., 2018. User-centric interdependent urban systems: using time-of-day electricity usage data to predict morning roadway congestion. Transportation Research Part C: Emerging Technologies, 92, 392-411. https://doi.org/10.1016/j.trc.2018.05.008
- Zhang, R.S., Zhang, J.Y., Long, Y., Wu, W.C., Liu, J.Y., Jiang, Y., 2021. Long-term implications of electric vehicle penetration in urban decarbonization scenarios: An integrated land use? transport? energy model. Sustainable Cities and Society, 68, 102800.

 https://doi.org/10.1016/j.scs.2021.102800
- Zong, F., Yue, S., 2023. Carbon emission impacts of longitudinal disturbance on low-penetration connected automated vehicle environments. Transportation Research Part D: Transport and Environment, 123, 103911. https://doi.org/10.1016/j.trd.2023.103911
- Zong, F., Zeng, M., Li, Y.X., 2024. Congestion pricing for sustainable urban transportation systems considering carbon emissions and travel habits. Sustainable Cities and Society, 101, 105198.

 https://doi.org/10.1016/j.scs.2024.105198